Kidney, Adrenal Gland, and Paraganglia

5

Xiaoqi Lin, Joseph F. Peevey, Ali Habib, Ronald Mora, and Ahsun Riaz

Kidney

Fine needle aspiration (FNA) has high sensitivity (80–100%) [1–3], specificity (91.9–100%) [1, 3, 4], positive predictive value (89.9%) [3], negative predictive value (94%) [3], and efficacy (92.2%) [3] in the diagnosis of malignant neoplasms of the kidney. As such, cytologic evaluation of renal lesions provides accurate and critical information for appropriate patient management.

Normal Renal Tissue

Renal Tubular Cells

Most epithelial cells seen in FNA smears of non-neoplastic kidney are renal tubular cells.

- They present as flat honeycomb tubules with parallel sharp borders, nests, or occasional gland-like structures (Fig. 5.1a).
- Tubular cells varying in size with indistinct cell borders and with scant to moderate amount of cytoplasm which is delicate or finely granular in texture.
- Tubular cells with small and round nuclei containing finely granular and evenly distributed chromatin, small or inconspicuous nucleoli, and smooth nuclear membrane.

Glomeruli

- Consist of large clusters of capillary loops and mesangial cells that are surrounded by Bowman capsule (Fig. 5.1b).
- Appropriate identification of this normal structure is critical so as to not misinterpret them as tumor cells.

Renal Cysts

Clinical

- Very common.
- Possibly congenital or acquired, single or polycystic, non-neoplastic or neoplastic, and benign or malignant.

Cytology of FNA or Touch Preparation of Core

The adequacy rate for FNA of renal cystic disease is estimated to be 56%, and the false negative rate 6.25% [4].

- Benign cysts: yield clear or pale, yellow fluid with few small, bland, or mildly atypical epithelial lining cells in small three-dimensional clusters; macrophages are seen in most cases. Additionally, neutrophils and occasionally Liesegang rings (three-dimensional laminated ring-like acellular structures) are also observed [5–7]. Epithelial cells seen within these benign specimens demonstrate round nuclei and ill-defined cell borders.
- Malignant cysts: generally bloody or "chocolate"-like fluid and the presence of atypical epithelial cells, macrophages, and lymphocytes [7]. Fluid from cystic renal cell carcinoma (RCC) may show features similar to those of benign cysts [7].

X. Lin (✉)
Northwestern University, Feinberg School of Medicine, Northwestern Memorial Hospital, Chicago, IL, USA
e-mail: xlin@northwestern.edu

J. F. Peevey
Department of Anatomic and Clinical Pathology, OSF St. Anthony Medical Center, Rockford, IL, USA

A. Habib
Department of Radiology, Northwestern University, Chicago, IL, USA

R. Mora
Department of Radiology, Section of Vascular and Interventional Radiology, Northwestern University, Chicago, IL, USA

A. Riaz
Department of Pathology, Northwestern Medicine, Chicago, IL, USA

R. Nayar et al. (eds.), *Atlas of Cytopathology and Radiology*, https://doi.org/10.1007/978-3-030-24756-0_5

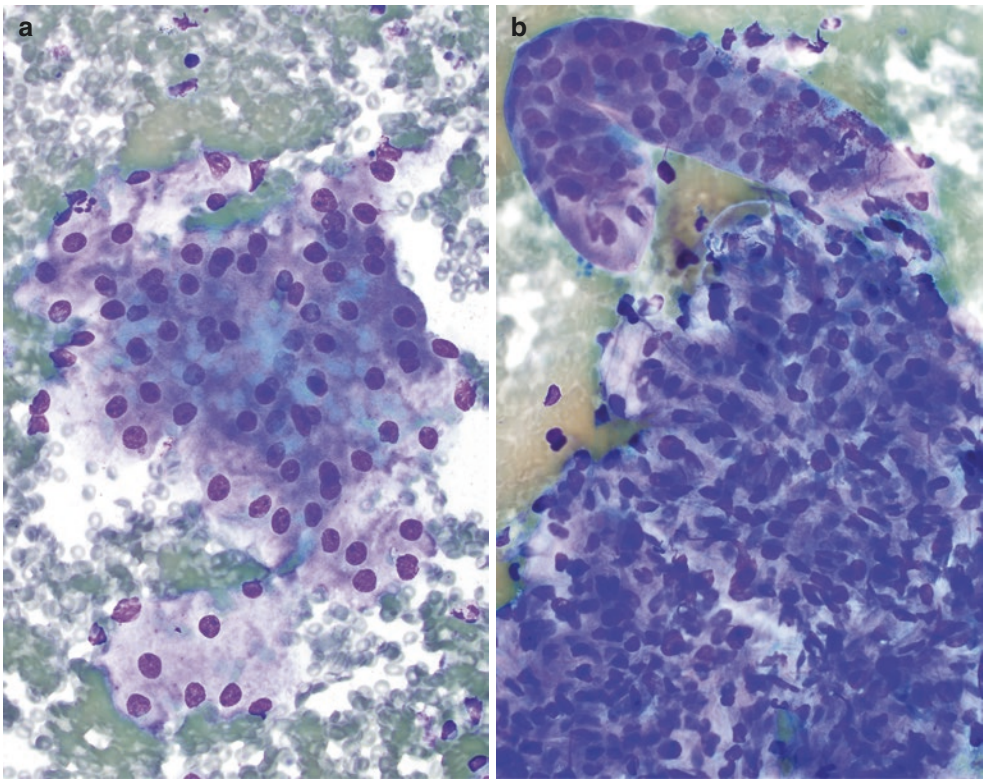

Fig. 5.1 Cytology of normal renal tissue. (**a**) Proximal renal tubule, Diff-Quik stain, 400×. (**b**) Glomerulus and proximal renal tubule, Diff-Quik stain, 400×

Comments

1. Benign epithelial cells with reactive atypia, especially with vacuolated cytoplasm; should be distinguished from RCC with cystic degeneration or cystic RCC.
2. Proximal renal tubule cells should be distinguished from oncocytoma or chromophobe type RCCs [8].
3. Chronic interstitial inflammation: Inflammatory changes can be seen in the kidneys, and the resultant distribution and nonspecific imaging characteristics may appear more nefarious in nature.
4. Renal infection: Pyelonephritis may result in wedge-shaped areas of hypoenhancement in the renal parenchyma. Renal abscesses demonstrate findings of abscesses elsewhere in the body, including a central area of fluid with an enhancing rim. On MRI, these restrict diffusion.

Benign Renal Neoplasms

Angiomyolipoma

Angiomyolipoma (AML) is a benign mesenchymal tumor composed of a variable proportion of adipose tissue, spindle and epithelioid smooth muscle cells, and abnormal thick-walled blood vessels. Angiomyolipomas are the most common benign tumors of the kidney and are more prevalent in the female population [9, 10].

Clinical

- Overall an uncommon entity, thought to represent 0.5–2% of all renal tumors. Some angiomyolipomas are associated with tuberous sclerosis [11–13].
- Male-to-female ratio is 1:4 to 1:10 in nontuberous sclerosis and 1:1 in tuberous sclerosis [11–13]. Average age is 45–55 years for patients without tuberous sclerosis and 25 to 35 for those patients with tuberous sclerosis [11–13].
- Usually asymptomatic. Patients may present with flank pain, hematuria, palpable mass, and retroperitoneal hemorrhage.

Radiology

Radiologic diagnosis of AML is complicated by the range of lipid content that an AML may contain, ranging from complete lack of fat to exhibiting macroscopic fat on cross-sectional imaging [9].

- On MRI, it is challenging to distinguish the microscopic fat of AMLs from that of clear cells on in-phase and out-of-phase T1-weighted imaging (Fig. 5.2) [14]. In addition, AMLs with lower lipid content are difficult to distinguish from papillary RCCs on T2-weighted images.
- Though AMLs are the most common benign tumor, there are abundant imaging pitfalls. Of note, if AML is >4 cm, prophylactic embolization is recommended because of the risk of rupture. Angiographically, AMLs have high vascularity and appear different from surrounding renal parenchyma.

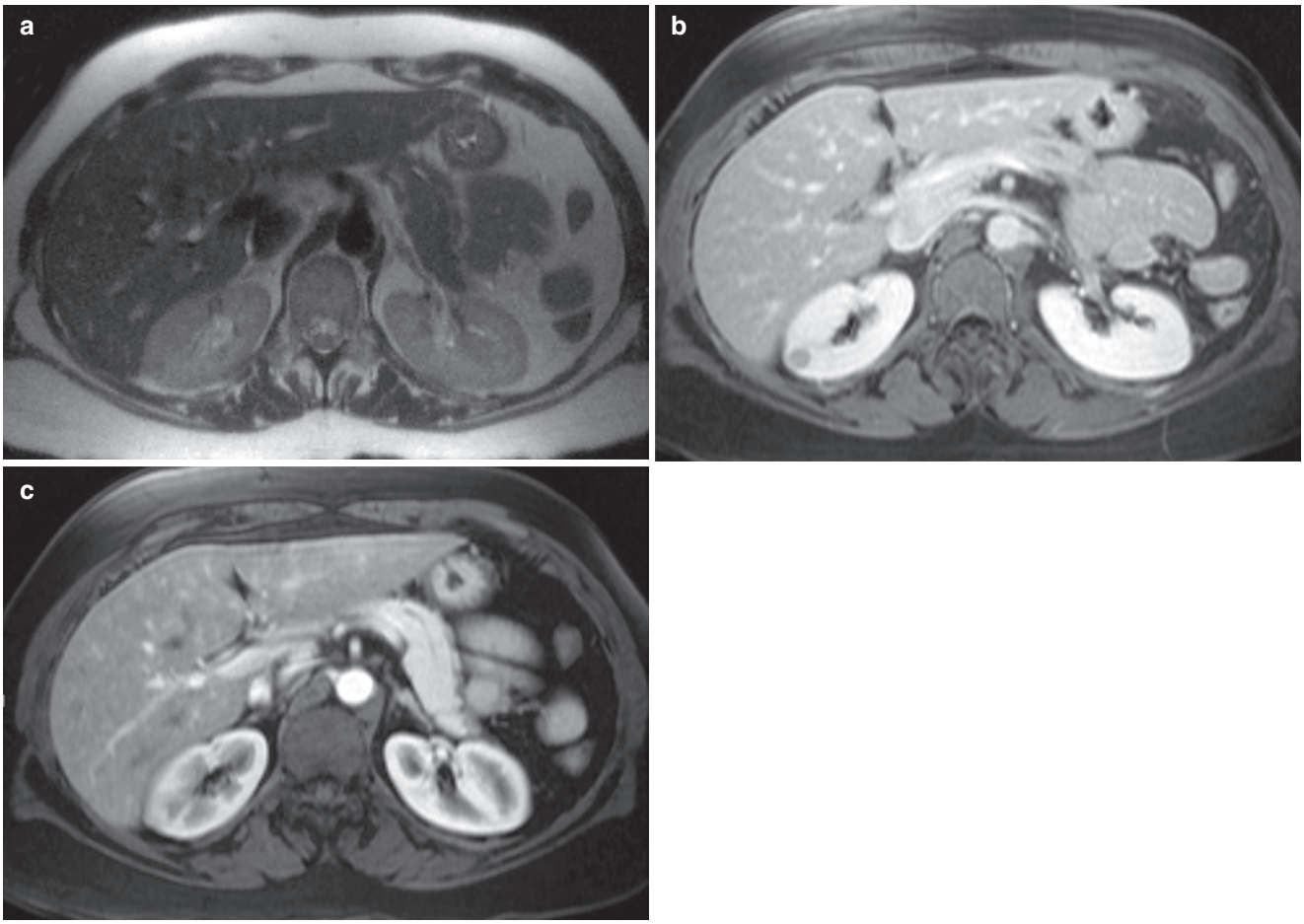

Fig. 5.2 Angiomyolipoma, radioimages. (**a**) Axial SHARP MRIs show a lesion in the right kidney that is isointense to the adjacent renal parenchyma. (**b**) Axial SHARP MRI at 17-minute delay shows a right renal lesion that is hypointense to renal parenchyma. (**c**) Axial SHARP postcontrast MRI sequence showing minimally increased ROI value consistent with enhancement

Cytology of FNA and Touch Preparation of Core

- Characteristically demonstrate a variable proportion of blood vessels and spindle and epithelioid smooth muscle spindled cells arranged in loosely cohesive or cohesive clusters as well as mature fat cells (Fig. 5.3) [15]. The nuclei of smooth muscle cells are oval to elongated with evenly distributed chromatin and no or inconspicuous nucleoli [15]. Naked nuclei are common. The cytoplasm is delicate and sometimes finely vacuolated [16]. Occasionally, smooth muscle cells and adipocytes may show atypia [15]. Mitoses and necrosis are absent [15]. Adipose tissue is not universally present [15].
- Fat necrosis can be seen, including histiocytes, multinucleated giant cells, and pleomorphic nuclei of adipocytes [17].

Comments

- Differential diagnosis includes perinephretic fat (misinterpreted as tumor adipose tissue), RCC (misinterpreted as epithelioid or atypical spindle smooth muscle cells), leiomyosarcoma (misinterpreted as atypical smooth muscle cells), and liposarcoma (misinterpreted as atypical adipocytes).
- These lesions are often sparely cellular, and positive staining of tumor cells can be very helpful in definitive diagnosis. Tumor cells are positive for melanocytic markers (HMB-45, CD63, tyrosinase, and Mart1/Melan-A), smooth muscle markers (smooth muscle actin, muscle-specific actin, desmin, and calponin), CD68, neuron-specific enolase, S-100, estrogen receptor, and progesterone receptor.

Oncocytoma

Oncocytoma is a benign renal epithelial neoplasm composed of large cells with mitochondria-rich eosinophilic cytoplasm; it is thought to arise from intercalated cells.

Clinical

- Approximately 3–7% of all renal neoplasms [18, 19].

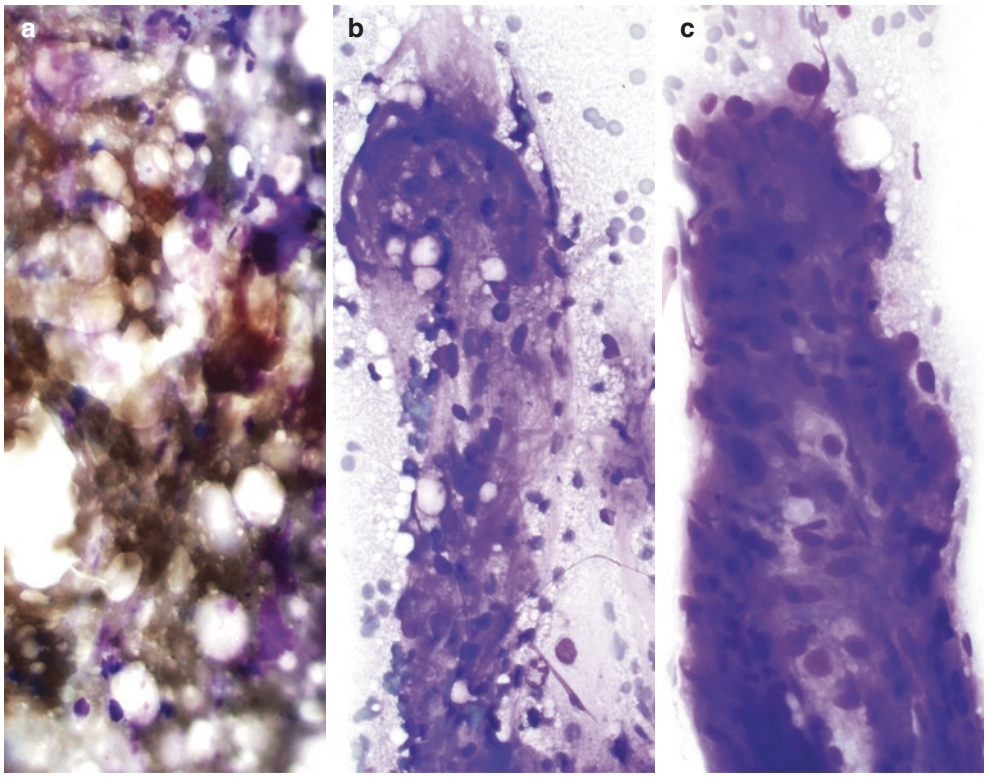

Fig. 5.3 Angiomyolipoma, cytology. (**a**–**c**) FNA biopsy of a renal mass, Diff-Quik stain, 400×

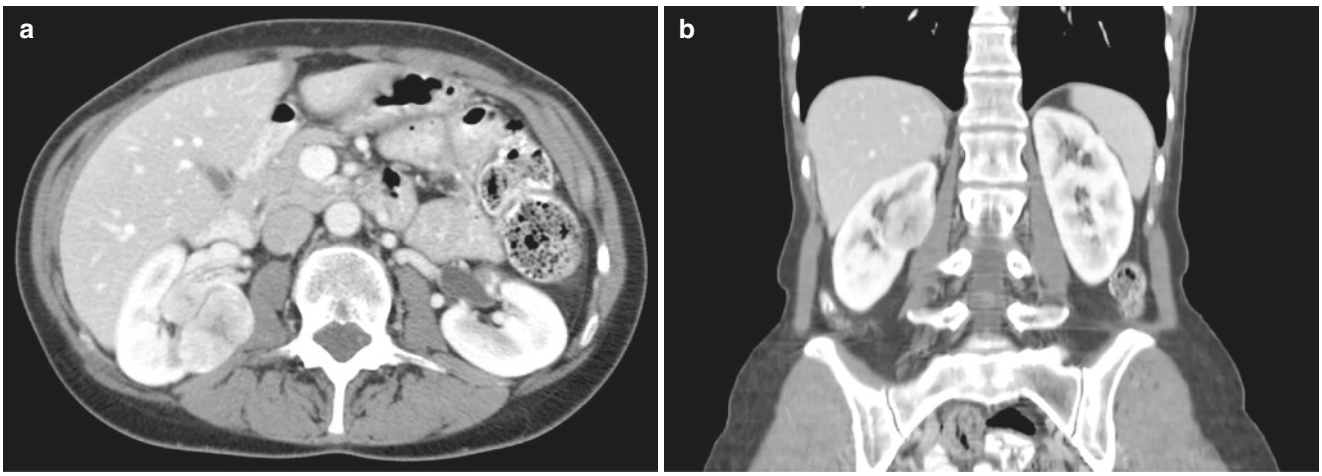

Fig. 5.4 Oncocytoma, radioimages. (**a**) CT scan shows a hyperenhancing mass in the middle pole of the right kidney which contains a central region of low density that may represent necrosis. (**b**) Coronal CT scan images show a hyperenhancing mass with a central region of necrosis

- Wide age range, with a peak in the seventh decade. Male-to-female ratio is 2:1 [20].
- Mostly asymptomatic, and a small number of patients present with hematuria, abdominal pain, and flank mass.
- Central stellate fibrous scar.
- Can be bilateral and multicentric and solid or cystic.

Radiology

- Oncocytomas have a pathologic origin similar to that of the chromophobe subtype of RCC, resulting in similar imaging features such as homogeneous features, spoke-wheel enhancement, and central stellate scar as shown in CT scan (Fig. 5.4) [21].

Cytology of FNA and Touch Preparation of Core

- Characteristically show single or small loose clusters of monotonous oncocytes (Fig. 5.5) [22].
- Oncocytes are large, polygonal or rounded with abundant and finely granular cytoplasm with well-defined cell borders [22].

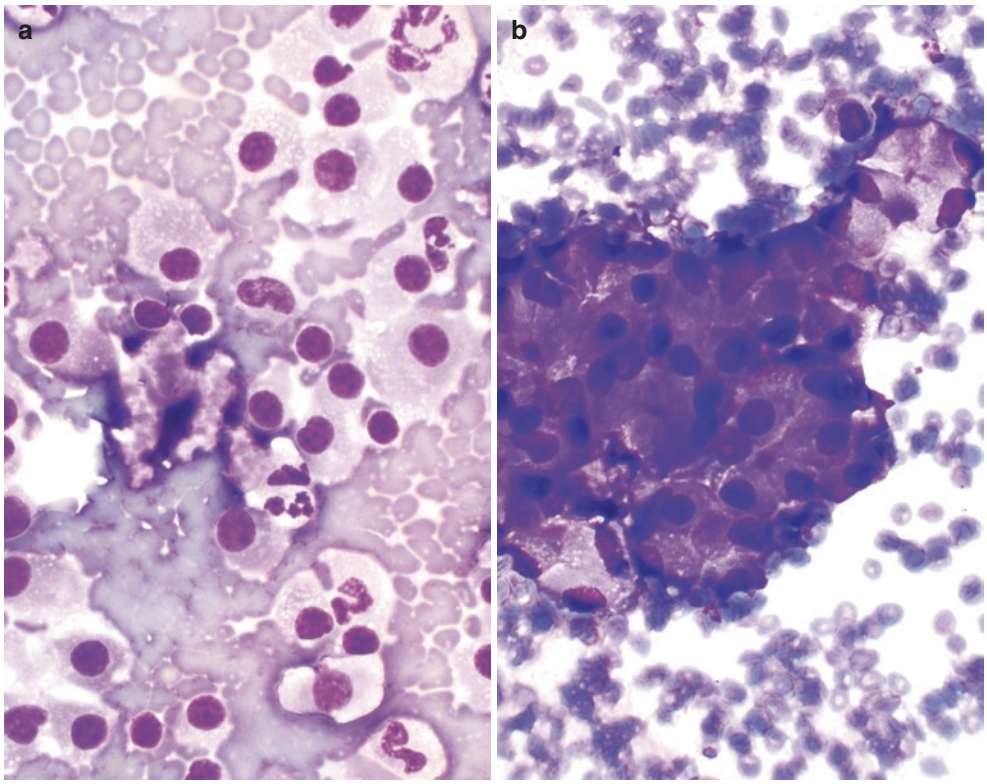

Fig. 5.5 Oncocytoma, cytology. (**a**, **b**) FNA biopsy of a renal mass, Diff-Quik stain, 600×

- The nuclei are usually small, round, regular, and centrally or eccentrically located (Fuhrman grade 2), with finely granular chromatin and no to conspicuous nucleoli [22, 23]. However, hyperchromatic or bizarre nuclei, binucleation, and nuclear enlargement can also be seen and are likely thought to represent degenerative change. Mitosis and necrosis are not usually observed.

Comments

- The differential diagnosis includes chromophobe RCC, clear cell RCC, normal renal tubular cells, and normal hepatocytes.
- The tumor cells are positive for CK7, epithelial membrane antigen (EMA), CD117, napsin A [24], E-cadherin, and S-100A1; they are less frequently positive for CD10 and alpha-methylacyl-CoA racemase (AMACR) [25]. Tumor cells are negative for the RCC antigen, vimentin [25]. There is no diffuse cytoplasmic Hale colloidal iron staining.

Malignant Renal Tumors

Renal Cell Carcinoma

RCC is a group of malignancies arising from the epithelium of the renal tubules. Based on the WHO classification (2016), it consists of familial renal cancer, clear cell RCC, multilocular cystic RCC, papillary RCC, chromophobe RCC, carcinoma of the collecting ducts of Bellini, renal medullary carcinoma, renal carcinomas associated with Xp11.2 translocations/TEF3 gene fusions, and clear cell papillary RCC [26]. Other tumors include RCC associated with neuroblastoma, mucinous tubular spindle cell carcinoma, papillary adenoma of the kidney, and unclassified RCC [27].

The clear cell subtype of RCC has worse outcomes relative to chromophobe and papillary subtypes, with a greater likelihood of metastasizing and presenting at a later stage [27–30]. The chromophobe subtype of RCC is less frequently seen than clear cell RCC and papillary RCC, with an incidence of approximately 5%. The papillary subtype of RCC is often discovered at a low grade stage and is small in size [30]. The size used to separate papillary RCC from papillary adenoma was increased from 0.5 cm to 1.0 cm in the 2016 WHO classification [27]. The five-year survival rate of papillary RCC is significantly better than that for clear cell, ranging from 82% to 92% [31, 32].

Clinical

- The ninth most common cancer in men and the fourteenth most common cancer in women [33] and >90% of all malignancies of the kidney [33].
- Male-to-female ratio is 2 to 3:1 [33, 34]. Its incidence increases steadily after 40 years of age [33].

- Clinical triad: hematuria, pain, and flank mass. Paraneoplastic endocrine syndromes can be seen [35].
- Can be solitary or cystic and single or multiple.

Radiology

- **RCC, clear cell type:** It typically exhibits heterogeneity caused by necrotic change, hemorrhage, or cystic change [32, 36]. It also exhibits features typical of most hypervascular lesions on CT (Fig. 5.6) [30].
- **RCC, chromophobe type**: The CT scan of chromophobe RCC shows a solid, homogeneous appearance with possible spoke-wheel enhancement or a stellate central scar (Fig. 5.7) [30].
- **RCC, papillary type**: The papillary subtype of RCC exhibits low signal intensity on T2-weighted MRI and is also hypervascular (Fig. 5.8).

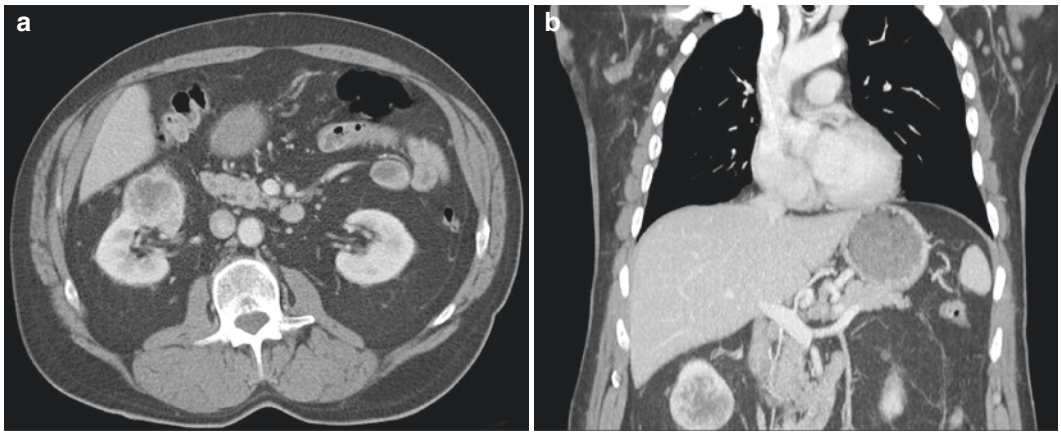

Fig. 5.6 RCC, clear cell type, radioimages. (**a**) CT scan shows an exophytic mass arising from the inferior pole of the right kidney. There is evidence of central necrosis. (**b**) CT scan on coronal view, in which the mass appears to have a central region of necrosis

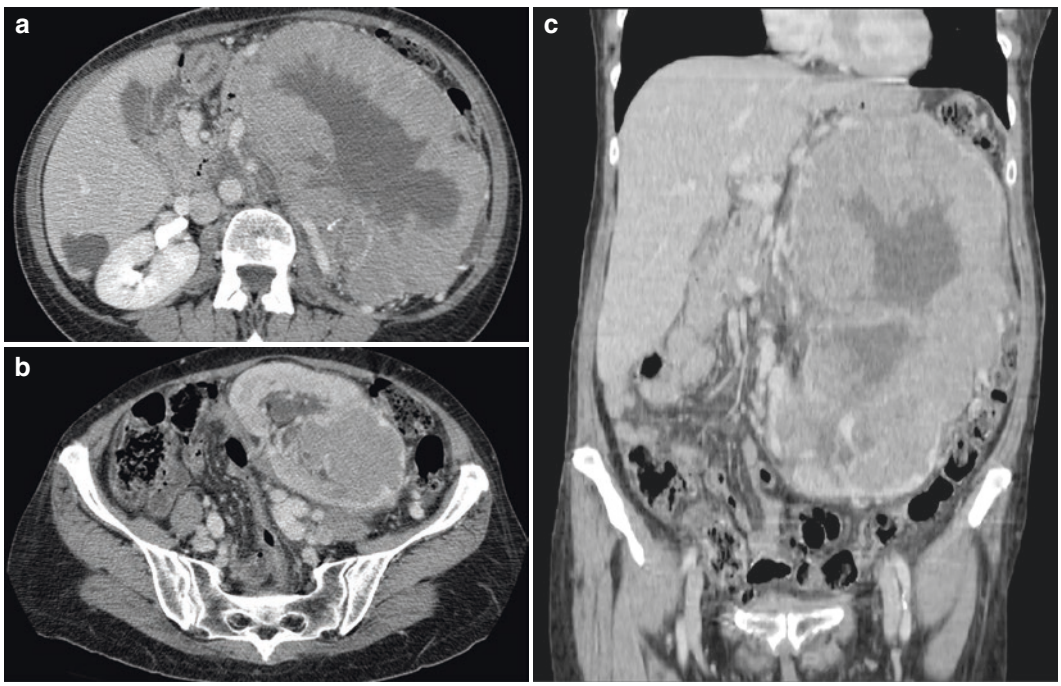

Fig. 5.7 RCC, chromophobe type, radioimages. (**a**) CT scan shows a large, heterogeneously enhancing multilobulated mass arising from the left kidney. Low density regions may represent necrosis or poorly enhancing tissue. There are coarse calcifications within the mass. (**b**) CT scan shows another view farther inferior to the large mass with associated compression and displacement of adjacent vessels. Hypoattenuating regions are again seen, possibly caused by necrosis. (**c**) CT scan shows that the true extent of the mass can be appreciated on the coronal image

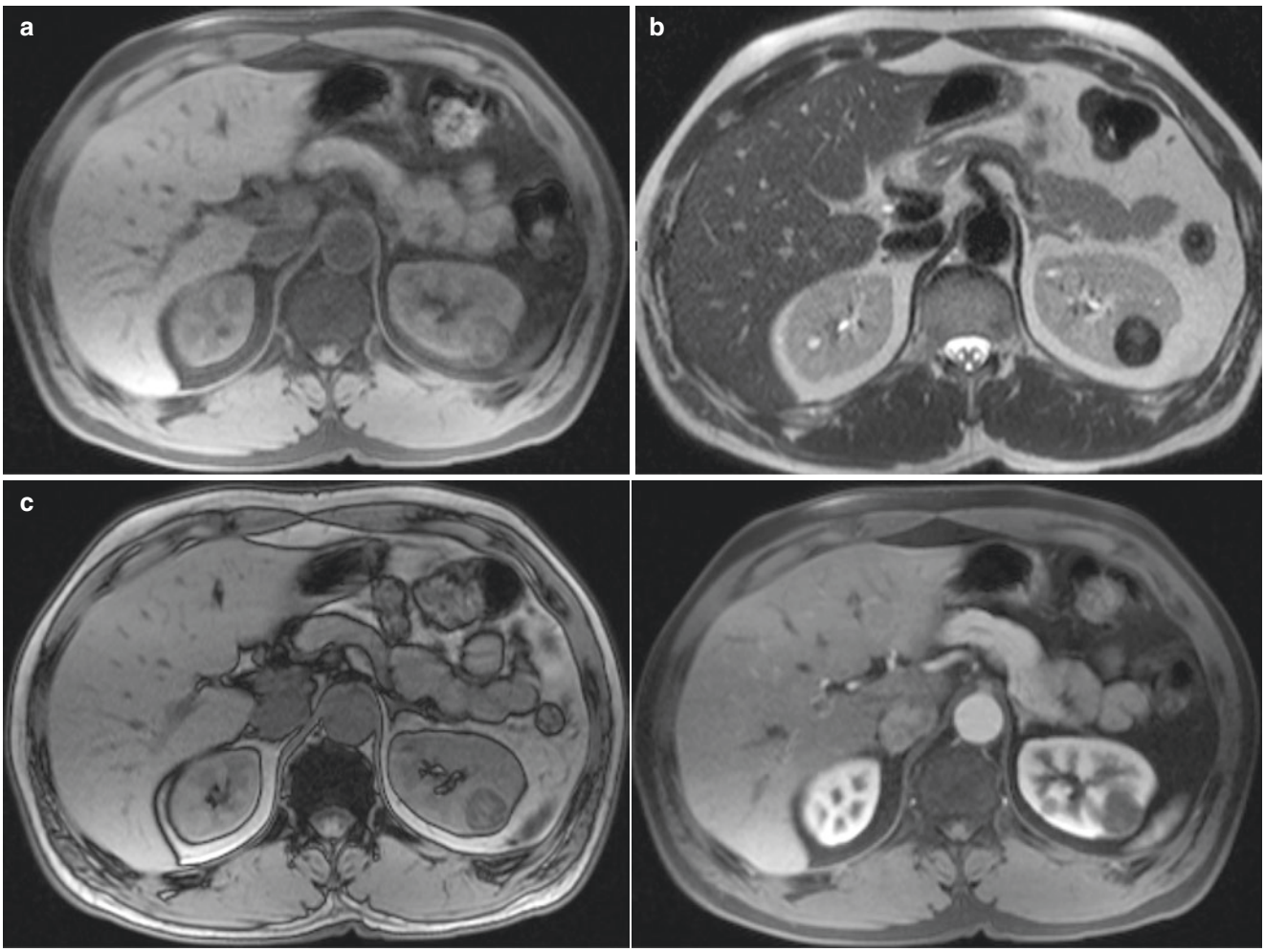

Fig. 5.8 RCC, papillary type, radioimages. (**a**) MRI (axial T1) shows a 2.5-cm lesion in the superior pole of the left kidney, which is slightly heterogeneous and showing decreased intensity on T1-weighted images. (**b**) MRI (axial HASTE) shows a hypointense lesion in the left kidney. (**c**) MRI (in-phase image) shows signal loss when compared to the out-of-phase images. (**d**) MRI (postcontrast) sequence of the lesion demonstrates mild early enhancement, which increases slowly over time

- **RCC, sarcomatoid differentiation**: The sarcomatoid differentiation can be found in any subtype of RCC. Thus, imaging features would probably be reflective of the subtype, although with aggressive features and resultant poor prognosis as shown in the CT scan (Fig. 5.9) [30].

Cytology of FNA and Touch Preparation of Core

- **RCC, clear cell type**: The most common cell type. Characteristically shows single, sheets, nests, papillary or floral-like groups, or three-dimensional clusters of clear cells with or without capillaries transversing the cells (Fig. 5.10a, b). The clear cells are large with low nuclear/cytoplasmic ratios. The cytoplasm is abundant, pale, wispy, delicate, reticulated, foamy, vacuolated, or granular. The nuclei vary from small to large, uniform to pleomorphism, bland to bizarre, smooth to irregular nuclear membrane, fine and evenly distributed chromatin to coarse and unevenly distributed chromatin, and no nucleoli to prominent nucleoli, depending on the grade of the tumor [6]. Intranuclear cytoplasmic invaginations, intracytoplasmic hyaline globules, naked nuclei, and multinucleated giant tumor cells can also be seen [6]. Necrosis, frothy background, fibrosis, hemosiderin, cholesterol, and fat may be seen in the background [6].
- **RCC, chromophobe type**: Characteristically shows clusters or single large cells with granular cytoplasm, well-defined cell borders, and a low-to-high nuclear/cytoplasmic ratio (Fig. 5.11a, b) [37]. The nuclei vary significantly in size, are often atypical, and have coarse and hyperchromatic chromatin, irregular nuclear membrane, smaller nucleoli, and peri-nuclear haloes [6]. Binucleation or multinucleation is frequently seen [6, 37].

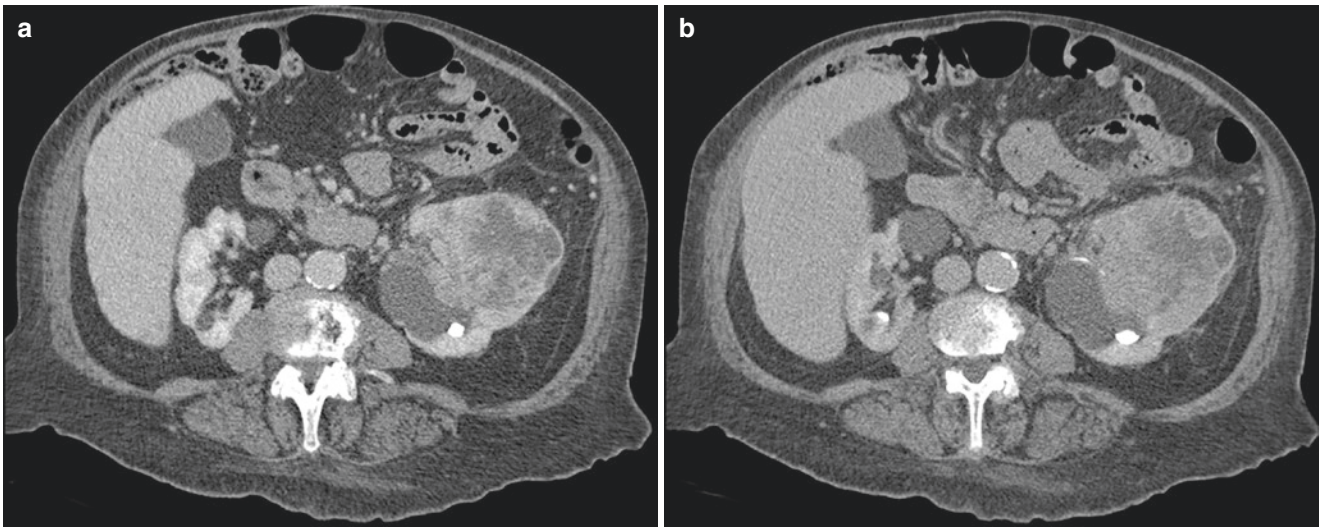

Fig. 5.9 RCC with sarcomatoid differentiation, radioimages. (**a**) CT scan shows a large, peripherally enhancing heterogeneous mass with suspected invasion of the proximal ureter as well as possible thrombosis of a renal vein branch. (**b**) CT again shows a large, heterogeneous mass obscuring the left upper pole and a portion of the renal pelvis

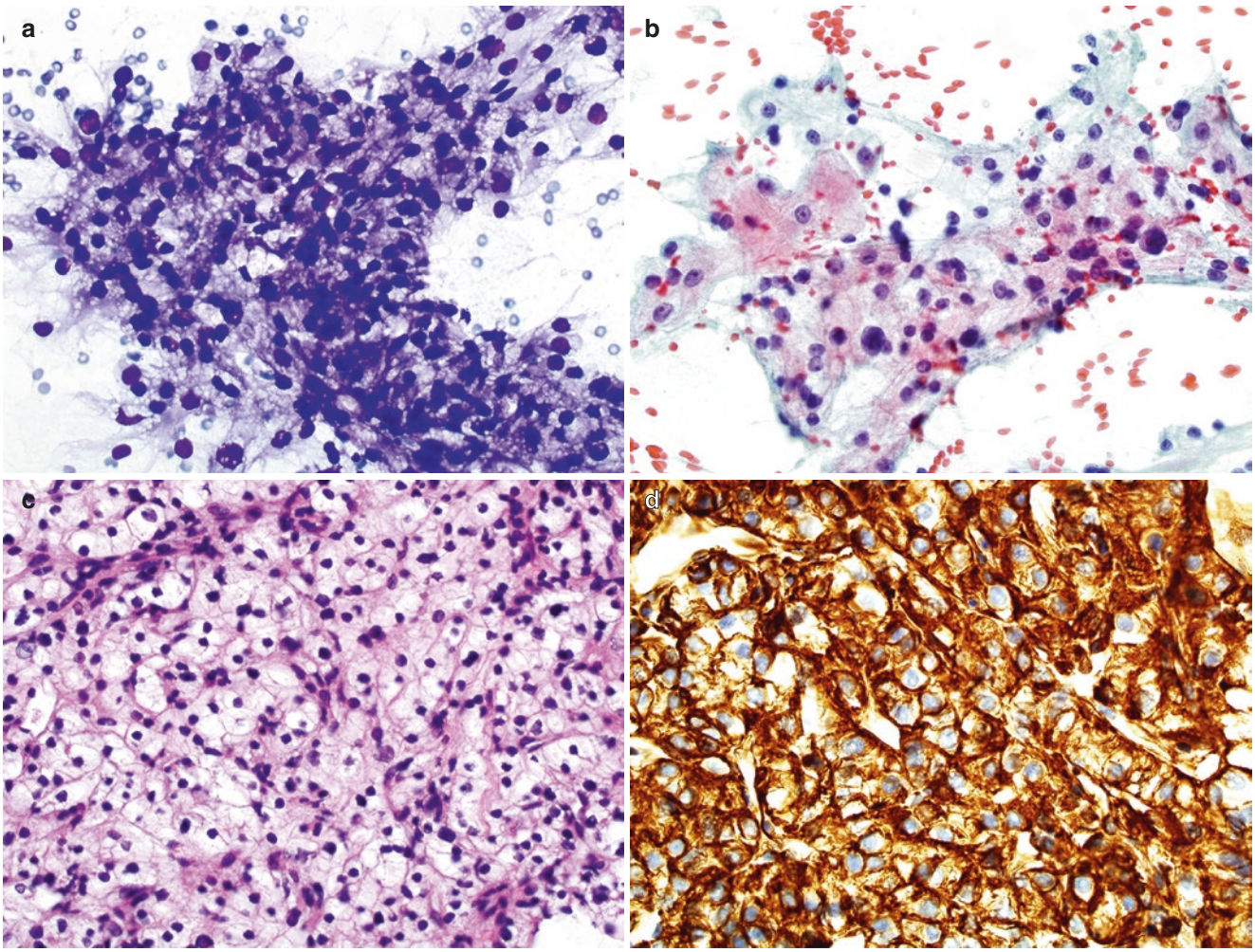

Fig. 5.10 RCC, clear cell type, cytology and histology. (**a**, **b**) Biopsy cytology of a renal mass, Diff-Quik stain (**a**) and Papanicolaou stain (**b**), 400×. (**c**) Histology of core, hematoxylin and eosin stain, 400×. (**d**) Immunostain for CA9, 400×

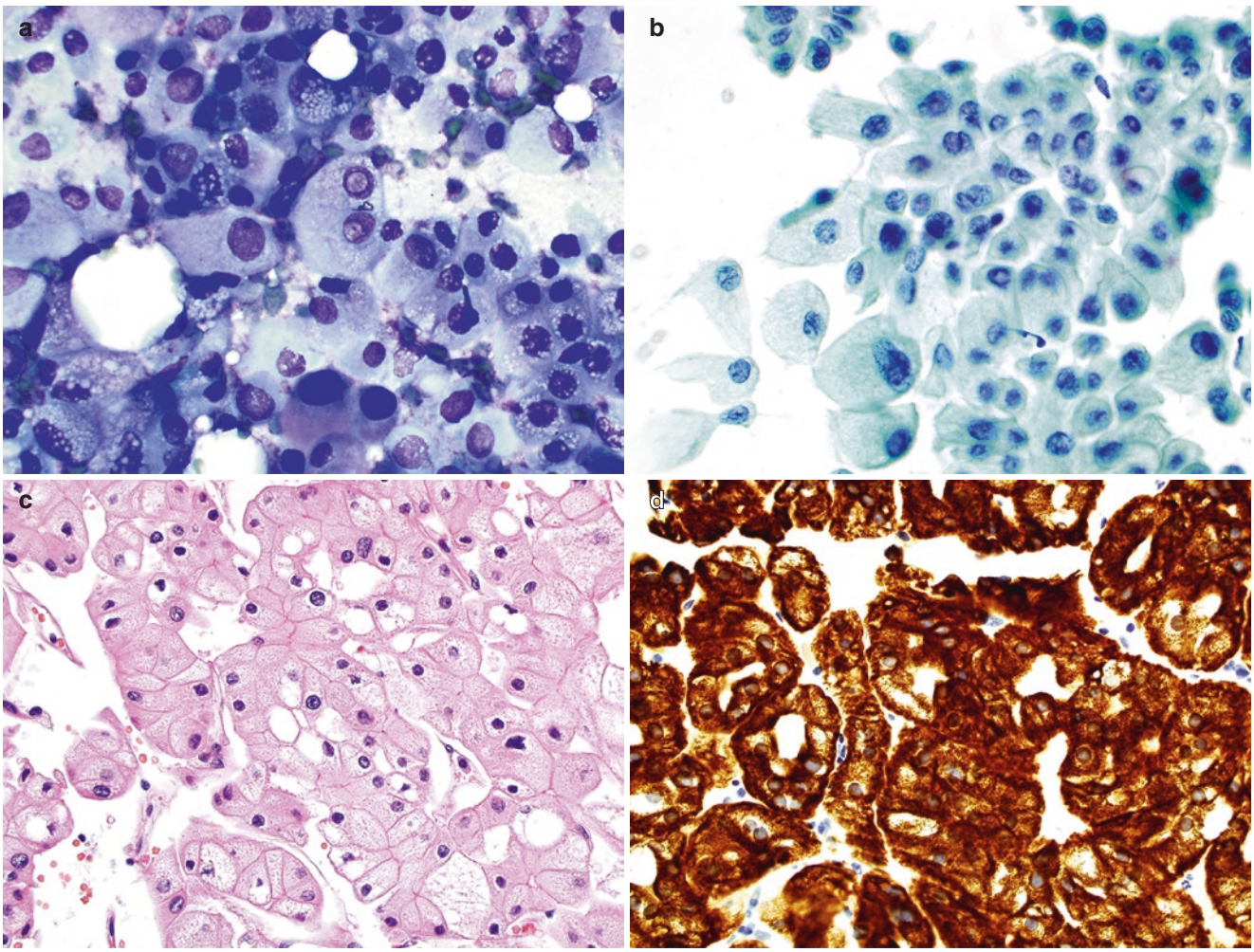

Fig. 5.11 RCC, chromophobe type, cytology and histology. (**a**, **b**) FNA biopsy of a renal mass, Diff-Quik stain (**a**) and Papanicolaou stain (**b**), 400×. (**c**) Histology of core, hematoxylin and eosin stain, 600×. (**d**) Immunostain for CK7, 600×

The cells are often referred to as "vegetable cells." Hemorrhage and necrosis are common, particularly in larger tumors.

- **RCC, papillary type**: Characteristically shows papillae composed of fibrovascular stalks surrounded by a layer of tumor cells, rounded spherules of tumor cells, single cells, and foamy or hemosiderin-laden macrophages (Fig. 5.12a). The fibrovascular stalks often contain histiocytes, with or without hemosiderin and/or lipid. The tumor cells are usually cuboidal to columnar. The nuclei are usually bland and uniform with fine chromatin, smooth to irregular nuclear membrane, small or inconspicuous nucleoli, and high nuclear/cytoplasmic ratios [6]. Pleomorphism, multinucleation, and mitotic figures are infrequent. Cytoplasm is scant and clear/pale in type 1 and abundant/eosinophilic in type 2. The tumor cells often contain hemosiderin pigment and may also contain intracytoplasmic vacuoles. Psammoma bodies, necrosis, and hemorrhage can be seen.
- **RCC, with sarcomatoid differentiation**: Characteristically shows discohesive spindle and pleomorphic cells with prominent nucleoli and delicate cytoplasm (Fig. 5.13a, b). Necrosis is frequently seen [16]. These cells show epithelial features by immunohistochemistry (IHC) and electron microscopy.
- **Collecting duct carcinoma**: Characteristically shows single or clusters of round or oval cells with tubule or papillary architectures. The nuclei are large and mildly atypical and have hyperchromatic and coarse chromatin and inconspicuous to prominent nucleoli. The cytoplasm is small to moderate in amount and finely granular with well-defined cell borders [38].

Histology of Core or Cell Block

- **RCC, clear cell type:** Sections show nests or sheets of large polygonal cells with capillary networks, foamy, clear, or granular cytoplasm, and centrally located nuclei

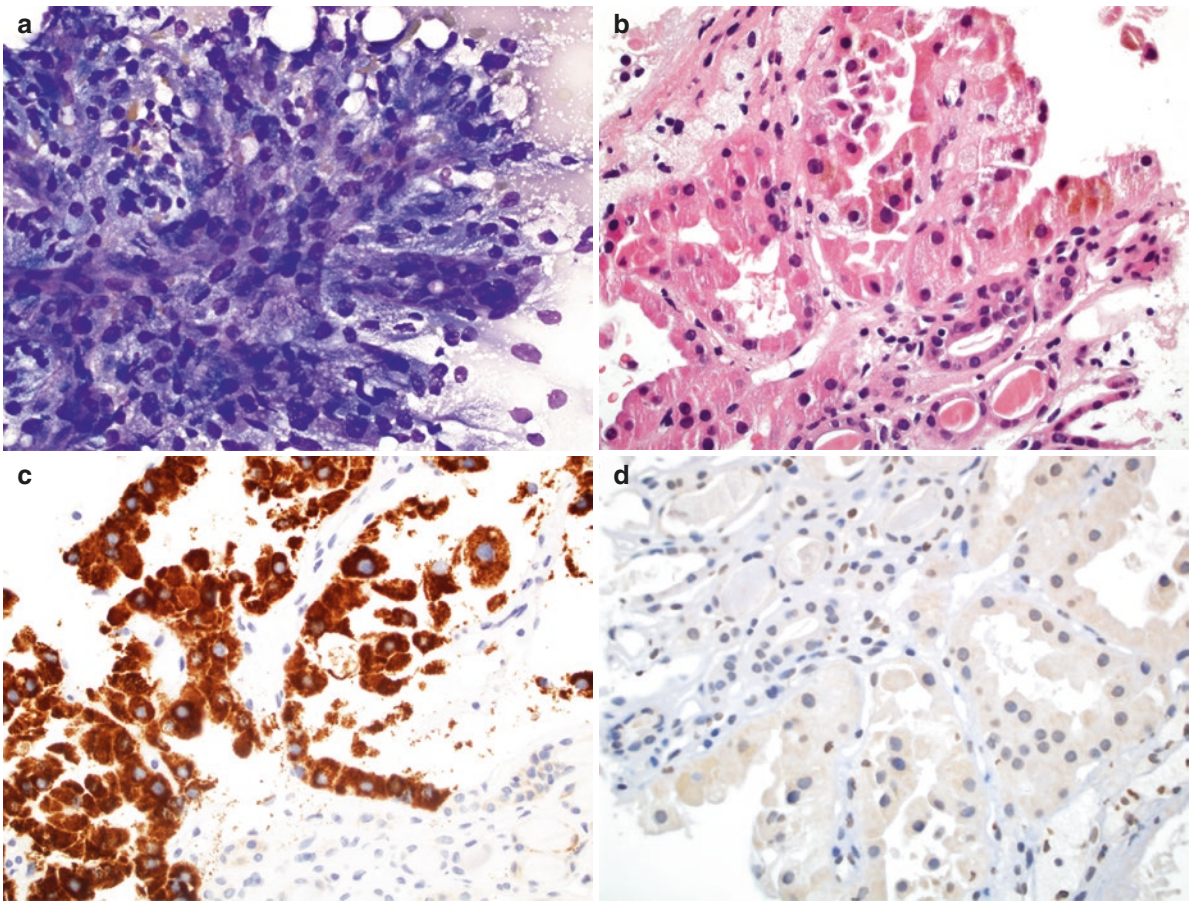

Fig. 5.12 RCC, papillary type, cytology and histology. (**a**) FNA cytology of a renal mass, Diff-Quik stain, 400×. (**b**) Histology of core, hematoxylin and eosin stain, 600×. (**c**, **d**) Immunostain for AMACR (**c**) and CA9 (**d**) 600×

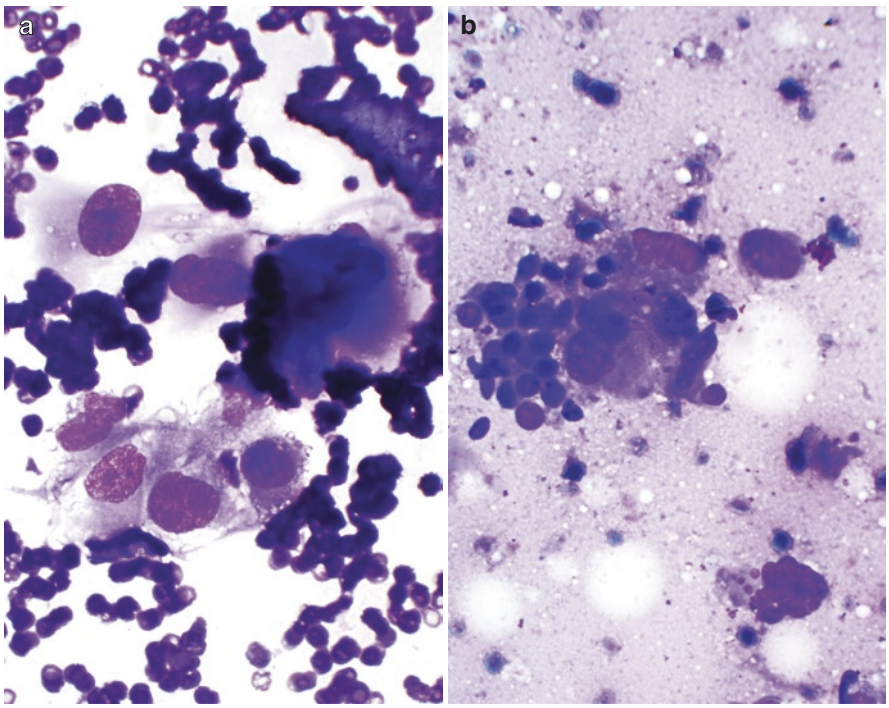

Fig. 5.13 RCC, high grade, with sarcomatoid feature. (**a**, **b**) FNA biopsy of a renal mass, Diff-Quik stain, 600×

that possibly contain nucleoli, depending on grading (Fig. 5.10c).
- **RCC, chromophobe type**: Sheets of polygonal cells with abundant granular cytoplasm, well-defined cytoplasmic borders, and round or oval nuclei with perinuclear halos (Fig. 5.11c).
- **RCC, papillary type**: Papillae lined by atypical epithelial cells with nuclear atypia with or without prominent nucleoli, depending on grading of tumor; scant to abundant eosinophilic, granular, or vacuolated cytoplasm, depending on type of papillary RCC (type 1 versus type 2) (Fig. 5.12b).

Comments

- For **clear cell RCC**, the differential diagnosis includes chromophobe RCC, papillary RCC, clear cell papillary RCC histiocytes [39], degenerated tubular cells, benign adrenal cortical cells, adrenocortical neoplasms, metastatic clear cell carcinoma from other primary tumors, and angiomyolipoma. Tumor cells are positive for cytokeratins (CAM5.2, CK19, AE1), RCC antigen, CA9 (Fig. 5.10d), CD10, EMA, napsin A [24], and vimentin and less frequently or weakly and focally positive for AMACR [AU: see earlier query Already added above], CD117, and E-cadherin [25]. Tumor cells are negative for CK7 and CK20.
- For **chromophobe RCC**, the differential diagnosis includes oncocytoma/oncocytic carcinoma, clear cell RCC, and benign proximal renal tubular cells [22]. Tumor cells are positive for pan-cytokeratins, including CK7 (Fig. 5.11d), EMA, and CD117, and less frequently positive for RCC antigen, napsin A [24], E-cadherin, and CD10. The tumor cells are negative for vimentin, AMACR, and CK20 [25]. There is diffuse cytoplasmic Hale colloidal iron staining [37].
- For **papillary RCC**, the differential diagnosis includes papillary adenoma (≤1 cm), well-differentiated papillary transitional cell carcinoma, clear cell RCC [27], and carcinoma of the collecting ducts of Bellini. Tumor cells are positive for cytokeratins (CAM5.2, AE1/AE3, and CK7), RCC antigen, CD10, EMA, AMACR (Fig. 5.12c), napsin A [24], vimentin, and S-100; they are less frequently positive for CD117 and CA9 (Fig. 5.12d) [40]. The type 1 tumor cells are negative for E-cadherin, and type 2 tumor cells are less frequently positive for E-cadherin [25].
- If FNA only shows sarcomatoid features, differential diagnosis includes leiomyosarcoma, angiomyolipoma, and spindle squamous cell carcinoma or urothelial carcinoma. The tumor cells are positive for both keratins and vimentin.
- For carcinoma of the collecting ducts of Bellini, tumor cells are positive for high molecular weight cytokeratins (34βE12, CK19), vimentin, CD15, EMA, and possibly mucin. Tumor cells are negative for CD10 and CD117 [25, 41].

Urothelial Carcinoma

Clinical

- Incidence is 1.2/100,000. Accounts for about 8% of all urothelial tumors [42].
- Predominantly found in older patients (mean age 70 years) with male-to-female ratio of 2:1 [42].
- Usually multifocal [42].
- Hematuria and flank pain are the chief presenting symptoms.

Radiology

- CT imaging features of urothelial carcinoma show possible thickening of the urothelial lining or a pelvi-calyceal filling defect (Fig. 5.14).
- Occasionally, these may present as masses much like RCC; however, location in the collecting system, slight enhancement, and the absence of necrotic or cystic change increase the likelihood that the lesion is more likely to be urothelial carcinoma [43].

Cytology of FNA and Touch Preparation of Core

- Low-grade urothelial carcinoma: characteristically shows papillary aggregates of minimally atypical urothelial cells.
- High-grade urothelial carcinoma: characteristically shows single or papillary aggregates of obvious malignant urothelial cells (Fig. 5.15). The nuclei are markedly pleomorphic and have coarse, irregular chromatin and prominent nucleoli. The cytoplasm is scant to moderate, glassy to dense, and occasionally vacuolated [6].
- Micropapillary architecture might be seen in urine cytology [44] and biopsy.
- Squamous differentiation, glandular cells, clear cells, or bizarre cells may be seen.

Comments

- Differential diagnosis includes reactive urothelial cells caused by stones, inflammation, and instrumentation, metastatic carcinoma, sarcoma, high grade RCC, and papillary RCC.
- Urothelial cells are positive for CK7, p63, p40, GATA3, CK20, CK5/6, K903, and thrombomodulin. GATA3 is more sensitive than traditional markers for conventional urothelial carcinoma and micropapillary urothelial carcinoma [45]. High-grade urothelial carcinoma tends to lose expression of p63 and p40, while it retains GATA3 expression [45]. Tumor cells are negative for napsin A [24].

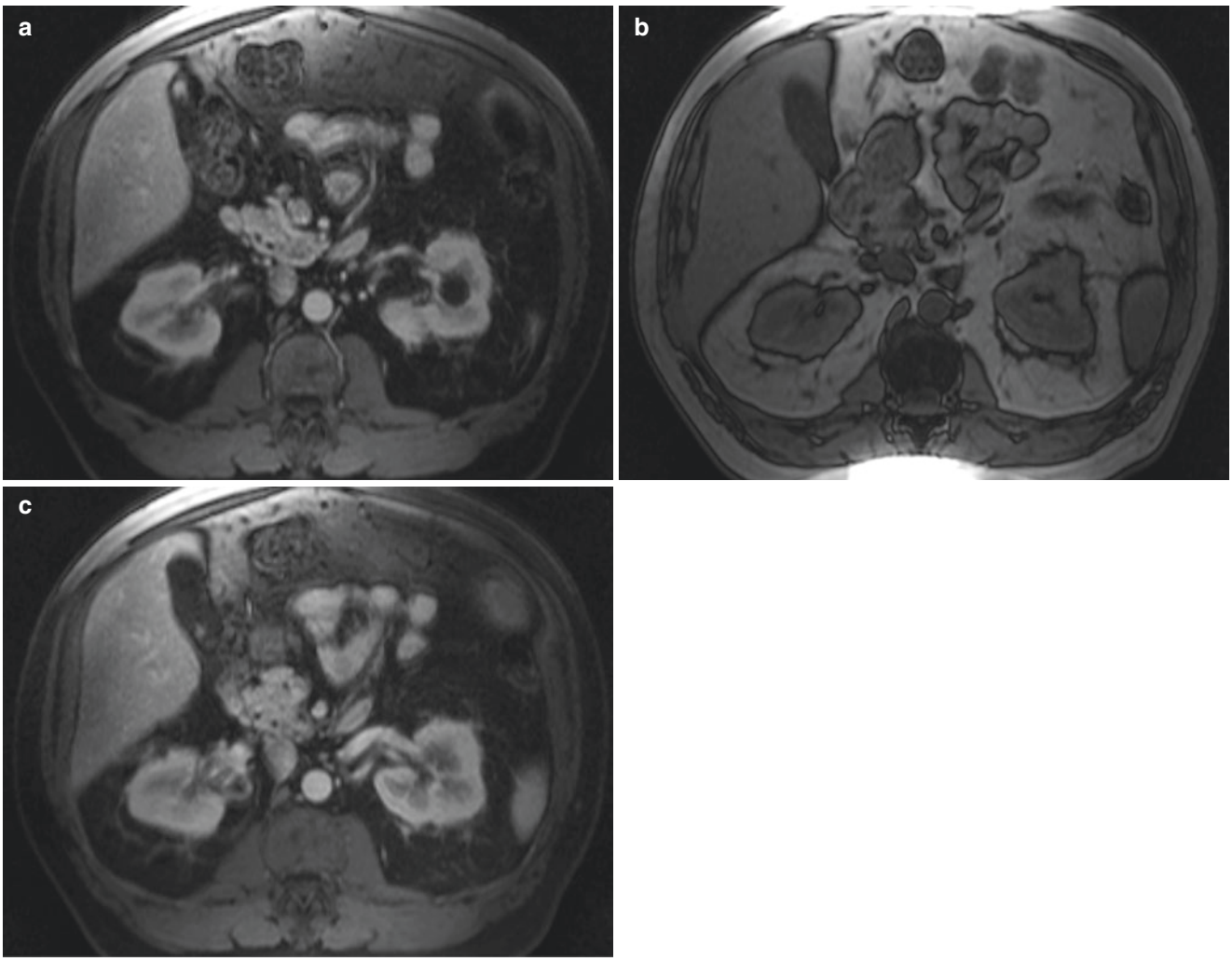

Fig. 5.14 Urothelial carcinoma, radioimages. (**a**) CT scan shows a large infiltrating mass occupying the upper half of the left kidney involving the central collecting system. Few pathologic lymph nodes are seen in the adjacent region. (**b**) Another CT scan view of the large left renal mass which enhances after contrast administration. (**c**) Early excretory phase of CT scan again shows an extensive, infiltrative mass

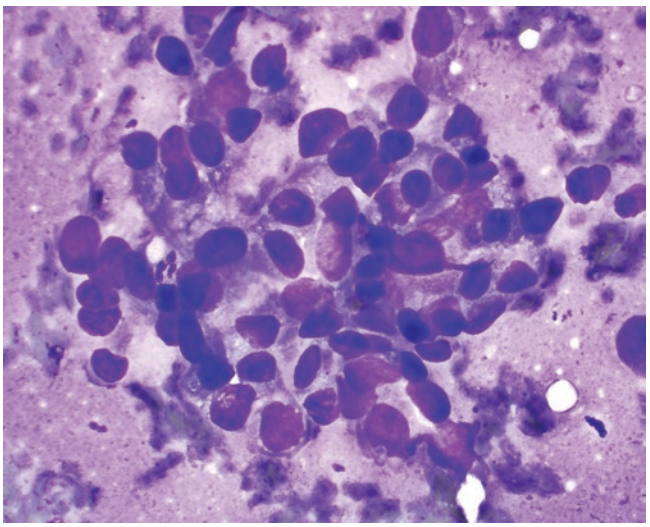

Fig. 5.15 Urothelial carcinoma, high grade. FNA biopsy of a renal mass from a patient with an enlarged retroperitoneal lymph node; Diff-Quik stain, 600×

Nephroblastoma (Wilms Tumor)

Nephroblastoma is a malignant embryonal neoplasm derived from nephrogenic blastemal cells that both replicates the histology of developing kidneys and often shows divergent patterns of differentiation [46].

Clinical

- 1/8000 children [46] and 85% of malignant renal tumors of children.
- Male-to-female ratio is 1:1 to 1:3 [46, 47]; 98% of cases are under 10 years old [46].
- Usually unilateral [46].
- Usually presents with an asymptomatic abdominal mass.

Cytology of FNA and Touch Preparation of Core

- Characteristically shows various combinations of dyscohesive three-dimensional sheets/groups of blastemal cells in all cases, epithelial cells in 60% of cases, stromal component in one third of cases, tubular differentiation in 26.6–85.7% of cases, and glomeruloid differentiation in 23.8–33.3% of cases [47–49]. Frequent mitoses can be seen [49].
- Blastemal cells are small- to medium-sized and round to oval. The cytoplasm is scant [48, 50]. The nuclei are round and hyperchromatic with fine chromatin, irregular nuclear membranes, and inconspicuous to distinct nucleoli [47–49]. Nuclear overlapping and molding can be seen [49]. In some cases the cells are strongly periodic acid-Schiff (PAS) -positive.
- The epithelial cells are larger than blastema cells [47, 48]. Nuclei are slightly larger than blastema nuclei, and the cytoplasm is more abundant [51]. Cohesive clusters of epithelial cells forming nests, glands, and tubules or glomeruloid bodies may be seen [47, 48].
- The stromal cells include spindle cells with a small amount of delicate cytoplasm and elongated, active nuclei (most commonly seen) set in a metachromatic, myxoid stroma [47, 48].
- Acute or chronic inflammatory cells, macrophages, and necrosis are common [50].

Comments

- The differential diagnosis includes a variety of other small blue cell tumors: embryonal rhabdomyosarcoma, Ewing sarcoma, lymphoma, desmoplastic small round cell tumor, and neuroblastoma [48].
- Tumor cells are positive for PAS, vimentin, neuron specific enolase (NSE), desmin, and cytokeratin. WT-1 is typical but not expressed in all nephroblastomas [46].

Metastasis

Clinical

- Metastases to the kidney are more common than primary renal neoplasms. Metastatic disease is the most common malignancy discovered in the kidney on autopsy [52].
- Common cancers that metastasize to the kidneys are lung, breast, colon, and malignant melanoma [53]. Several primary renal tumors (mucin-positive RCC, urothelial carcinoma, collecting duct carcinoma) can be mistaken for metastatic lesions based on cytomorphology alone. In these instances, ICH staining is very helpful.

Radiology

- Both primary and secondary lymphomas of the kidney can be seen; however, secondary lymphoma is significantly more common. If a patient has widespread lymphoma, direct extension from adjacent lymph nodes or hematogenous spread can result in renal involvement. The elevated nucleus-to-cytoplasmic ratio and the large number of cell results restricted diffusion on MRI, along with intermediate signal intensity on both T1- and T2-weighted sequences.
- On CT scan, the nephrographic phase allows for maximal spatial resolution to aid in evaluation for metastatic disease (Fig. 5.16) [54]. Renal melanoma is rare. However, when it does occur, it usually follows the features of melanoma, which are nonspecific on ultrasound and CT. However, on MRI, there is a T1 hyperintense signal and T2 hypointense signal. In addition to these findings, there is hyperenhancement.

Cytology and Histology

- Cytomorphology/histomorphology differ, depending on type of metastatic malignancy.
- Comparison with morphology of primary malignancy is important.
- A panel of immunostains can be performed to confirm the diagnosis.

IHC for napsin A has been widely used to support a diagnosis of lung adenocarcinoma with reported high sensitivity [24]; however it is also expressed in many renal neoplasms [24], therefore, care should be taken when trying to separate a renal primary from a lung primary using Napsin.

Adrenal Glands

Use of FNA biopsy for incidentally discovered adrenal masses or "incidentalomas" is controversial [55–57]. Incidental findings can be seen in approximately 0.4–4.4% of all CT studies [58, 59]. Adrenal lesions are often identified on cross-sectional imaging in symptomatic and asymptomatic patients. Because of the uncertain nature of certain adrenal imaging findings, the utility of radiologic and pathologic correlations is high in this clinical scenario. By classifying key features of different biopsy-proven pathology, imagers will find that radiologic findings can potentially streamline downstream clinical care [56]. Using FNA may make it difficult in some cases to distinguish benign from malignant adrenal cells with certainty [60]. However, reports have stated that image-guided FNA cytology is a safe and sensitive procedure and should be performed in all patients with incidentally discovered adrenal masses with high sensitivity (83.3–100%) [61, 62], specificity (96.3–100%) [61,

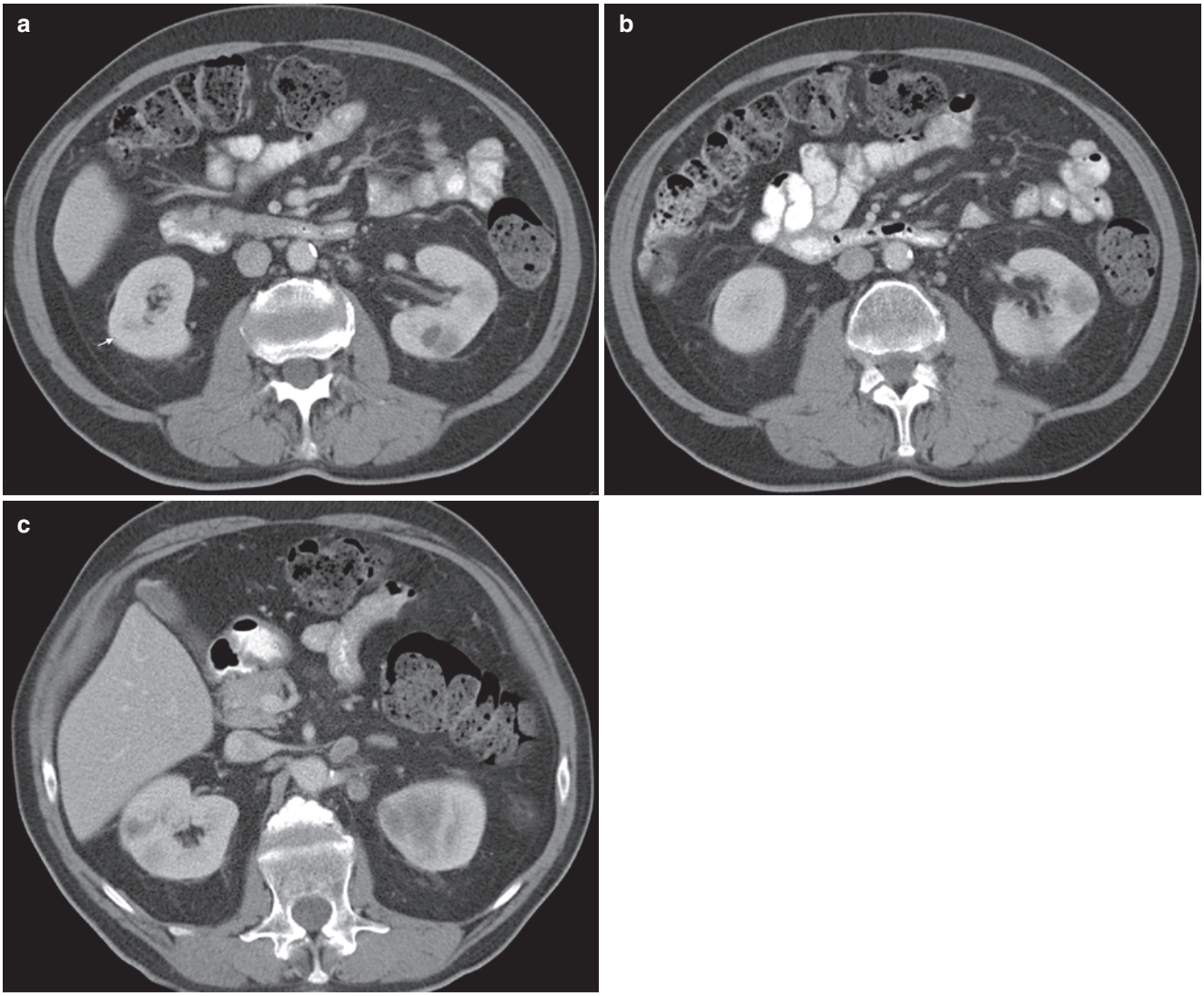

Fig. 5.16 Metastatic malignancy to the kidney, radioimages. (**a**) CT scan shows bilateral, poorly defined hypodense masses scattered throughout both kidneys. The largest is a hypodense mass in the upper pole of the left kidney. (**b**) Additional CT scan view of hypodense lesions within both kidneys. (**c**) Additional CT scan view of hypodense lesions within both kidneys

62], positive predictive value (95.8–100%) [61, 62], negative predictive value (100%) [62], and accuracy (97.6%) [62]. FNA biopsy may cause fatal hypertensive crisis or hemorrhage in pheochromocytoma, therefore biochemical testing should be performed before biopsy of adrenal masses. Complications include hypertension, hematoma of the liver, thorax, and duodenum [50], and pneumothorax [56].

Adrenal Epithelial Cells

Cytology of FNA or Touch Preparation

- Adrenal cortical cells present ias cords, small aggregates, or singly (Fig. 5.17). The cells are generally uniform and polygonal, with small to moderate, uniform and round nuclei with granular chromatin and a distinct nucleolus. Marked nuclear atypia, pleomorphism,

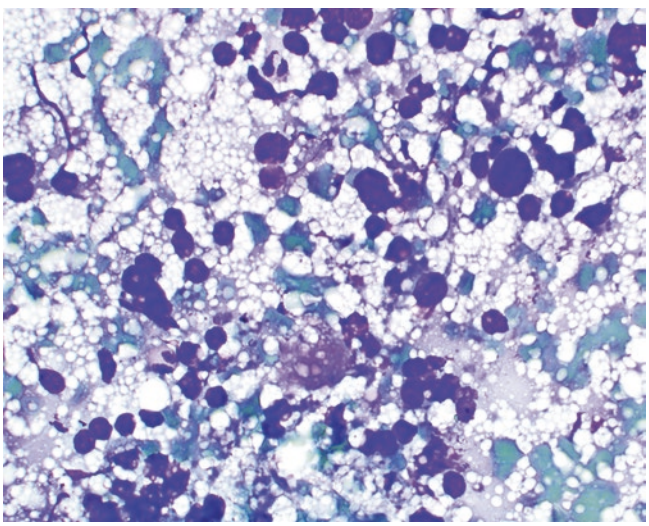

Fig. 5.17 Benign adrenal cortex cells, cytology; Diff-Quik stain, 600×

multiple large nucleoli, and binucleation may be seen. Naked nuclei are common. The cytoplasm is abundant, finely vacuolated or finely granular, and delicate with frayed cell borders.
- Adrenal medulla cells are polygonal and variable in size and shape. The nuclei have granular chromatin and a distinct nucleolus. The cytoplasm is finely granular and frequently contains lipofuscin. Intracytoplasmic hyaline globules are also commonly observed.

Inflammatory Lesions

Clinical

- When FNA is utilized to exclude a neoplasm, an inflammatory lesion may be encountered. Since it may or may not be due to infectious organisms; triage for cytologic material for microbiology studies should be be utilized.

Radiology

- It is often challenging to distinguish between inflammatory changes and neoplastic lesions in the adrenal gland.
- The overall MRI features are nonspecific, bringing adenomas, adrenal hematomas, or infection within the realm of possibility. Upon biopsy, the lesion often is found to be inflammatory change (Fig. 5.18).

Cytology of FNA and Touch Preparation of Core

- The presence of inflammatory cells (neutrophils, lymphocytes, macrophages) and benign adrenal cells (Fig. 5.19). Necrosis and/or granulomas may be seen.

Comment

- Special stains and microbiologic cultures should be performed to detect and definitively identify organisms (e.g., bacteria, mycobacteria, viruses, fungi).

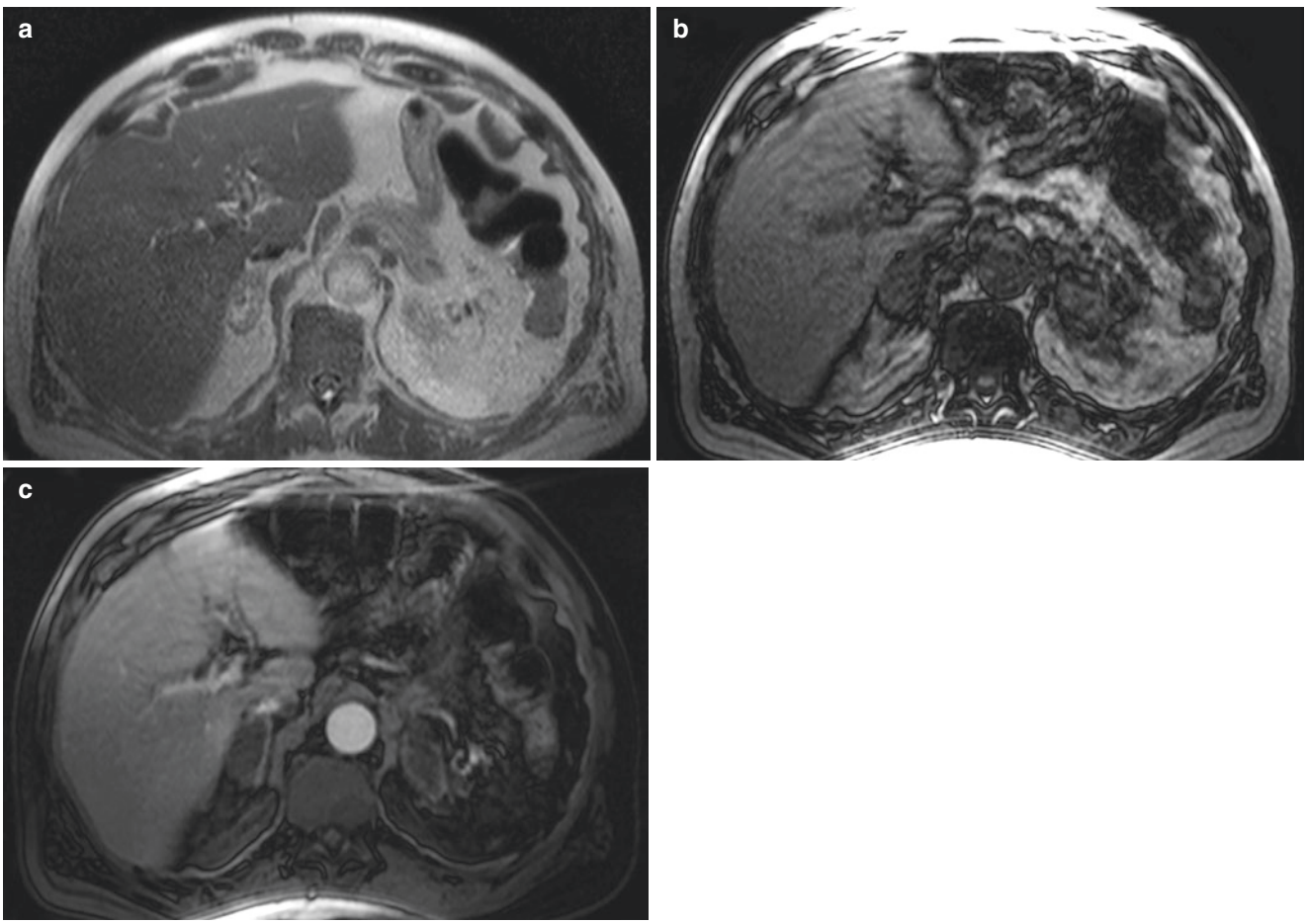

Fig. 5.18 Adrenal gland, inflammation, radioimages. (**a**) MRI (T1-weighted image) of the right adrenal nodule demonstrates heterogeneous signal intensity on precontrast images. (**b**) MRI (out of phase image) shows no definitive loss of signal on out of phase images. (**c**) MRI (postcontrast image) shows peripheral enhancement with low signal intensity

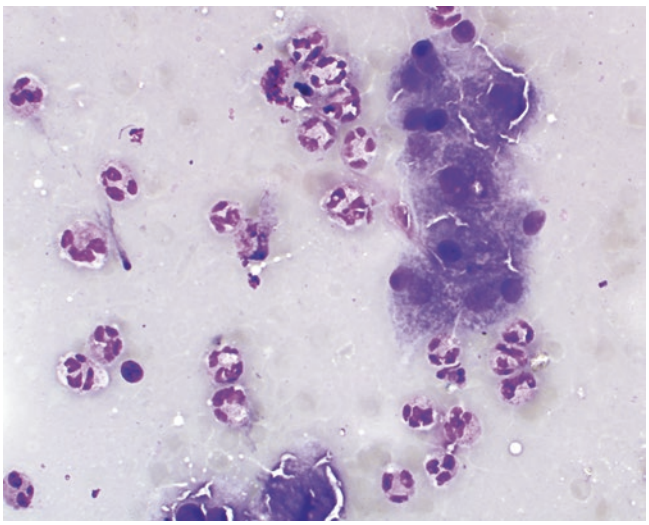

Fig. 5.19 Adrenal gland, inflammation, cytology. FNA biopsy of a lesion in the adrenal gland shows abundant neutrophils; Diff-Quik stain, 600×

Benign Adrenal Neoplasms

Adrenal Myelolipoma

Myelolipomas are benign tumors that exhibit macroscopic fat that is prominent on both CT and MRI [63]. Myelolipomas have a prevalence of 0.08–0.2% [64]. Patients are usually asymptomatic, and rarely myelolipomas may result in functional symptoms [65].

Clinical

- Uncommon benign neoplasm, 2.5% of primary adrenal tumors [66].
- In middle to late adult life without sex predilection.
- No clinical symptoms.

Radiology

- Macroscopic fat; on MRI exhibits decreased signal intensity on fat-saturated T2-weighted images and increased intensity on T1-weighted sequences (Fig. 5.20).

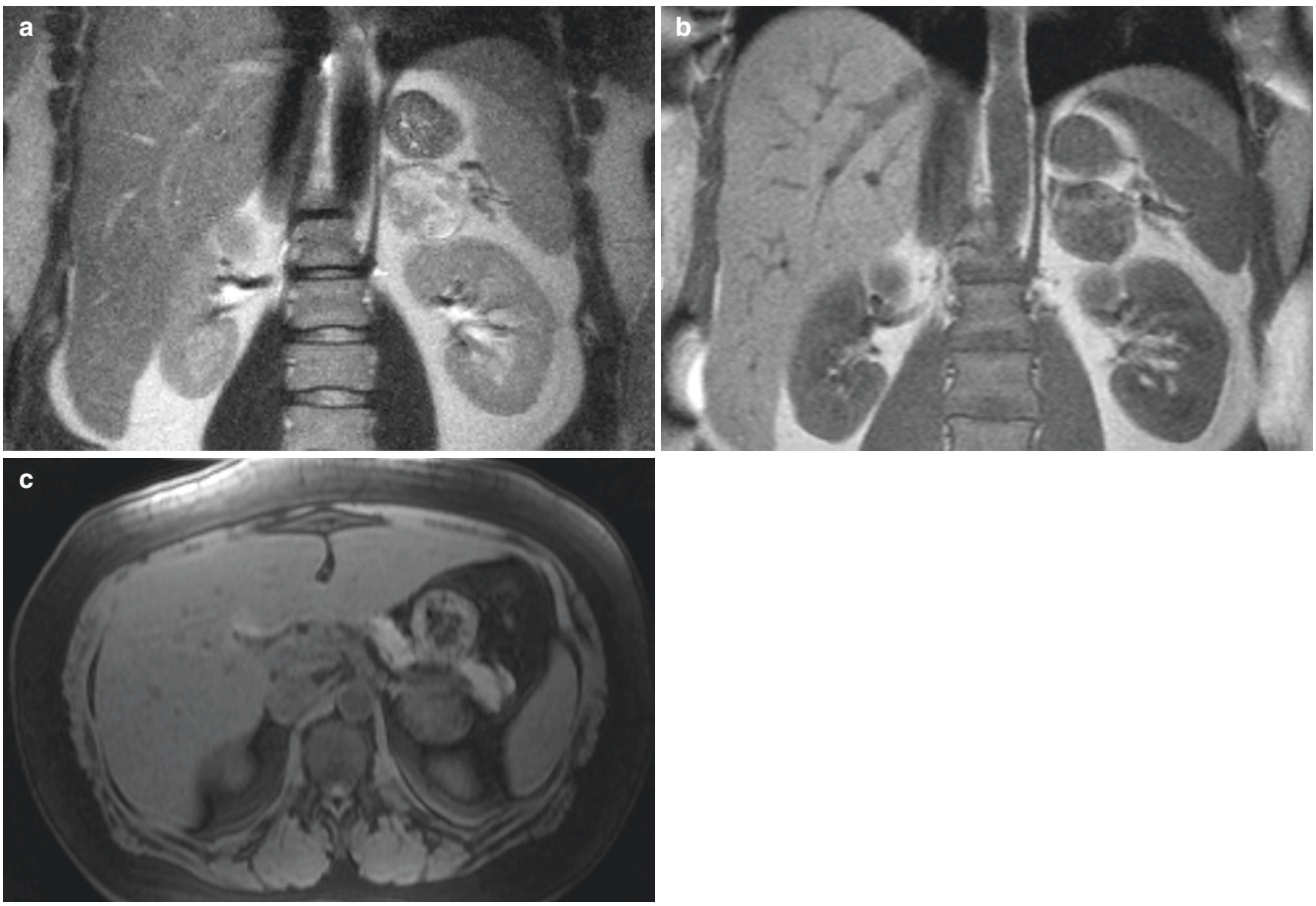

Fig. 5.20 Adrenal myelolipoma, radioimages. (**a**) MRI (T2-weighted image) shows an approximately 4-cm mass in the left adrenal gland with heterogeneous signal intensity, also shown to be mildly hyperintense on T2-weighted images. (**b**) MRI (in-phase image) is shown above, and there is heterogeneous loss of signal intensity on subsequent out-of-phase images. (**c**) MR (axial SHARP) sequence image shows increased peripheral signal intensity

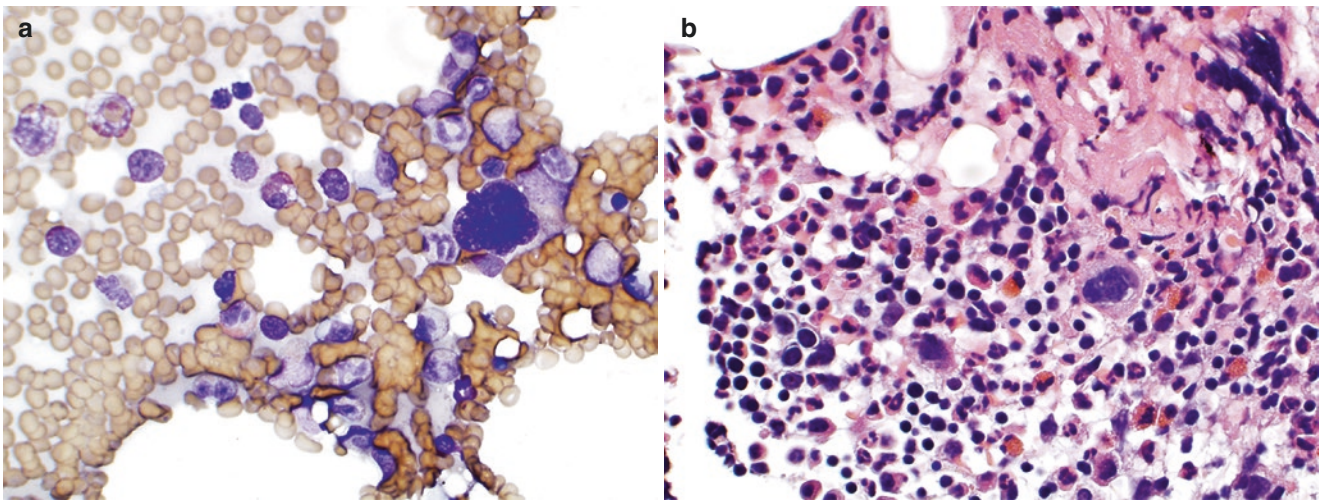

Fig. 5.21 Adrenal myelolipoma, cytology and histology. (**a**) Biopsy cytology of an adrenal lesion, Diff-Quik stain, 600×. (**b**) Histology of core, hematoxylin and eosin stain, 600×

Cytology of FNA and Touch Preparation of Core

- Characteristically bone marrow hematopoietic cells (megakaryocytes, myeloid blasts, premyelocytes, myelocytes, and erythrocytic precursors) and mature adipose tissue in variable proportions are present (Fig. 5.21a) [67].

Histology of Core

- Bone marrow trilineage hematopoiesis and adipose tissue (Fig. 5.21b).

Comments

- Special stains (chloroacetate esterase, myeloid peroxidase) or immunostains (factor VIII) can also confirm the myeloid nature of the immature cells.
- The differential diagnosis includes well-differentiated liposarcoma and hematopoietic tumors.

Adrenal Cortical Adenoma

Adrenal adenomas are the most common benign tumor of the adrenal gland with a prevalence of up to 8.9% [59].

Clinical

- Incidence on autopsy series is 1.5–7% and increases with age [68].
- No sex predilection [69].
- Eighty-five percent of adenomas are nonfunctional [68].

Radiology

The increased vascularity and elevated lipid content of adrenal adenomas results in certain key imaging characteristics on CT and MRI.

CT Scan

- Density evaluation of an adrenal lesion is highly sensitive and specific, since 70% of adrenal adenomas contain intracellular fat.
- On noncontrast imaging, <0 Hounsfield Units has a 100% specificity for adrenal adenoma and <10 Hounsfield Units has 98% specificity for adrenal adenoma. Lipid-poor adenomas are more difficult to diagnose because the CT density increases and approaches that of soft tissue. For lipid-poor lesions, the contrast washout rate can be calculated at CT.
- Adenomas typically have rapid contrast washout, whereas non adenomas tend to wash out more slowly (Fig. 5.22a, b). A 15-minute postcontrast washout image has great sensitivity (Fig. 5.22c). A >60% absolute washout and >40% relative washout are consistent with adrenal adenoma.

MRI

- The protons in fat and water differ and respond differently to sequences, with resultant weakening of signal intensity on out-of-phase sequences.
- Chemical shift imaging is an important parameter when assessing adrenal adenomas. The presence of fat within the lesion does not assure benignity, for many malignant lesions such as clear cell RCC and pheochromocytomas contain significant lipid content [70].
- Adrenal adenomas do not demonstrate restricted diffusion.

Cytomorphology of FNA and Touch Preparation of Core

- Presence of loose aggregates, fascicles, or microacini of polygonal cells (Fig. 5.23) [62, 71]. The specimen is less cellular than adrenal cortical carcinoma, and cells are smaller than carcinoma [62].

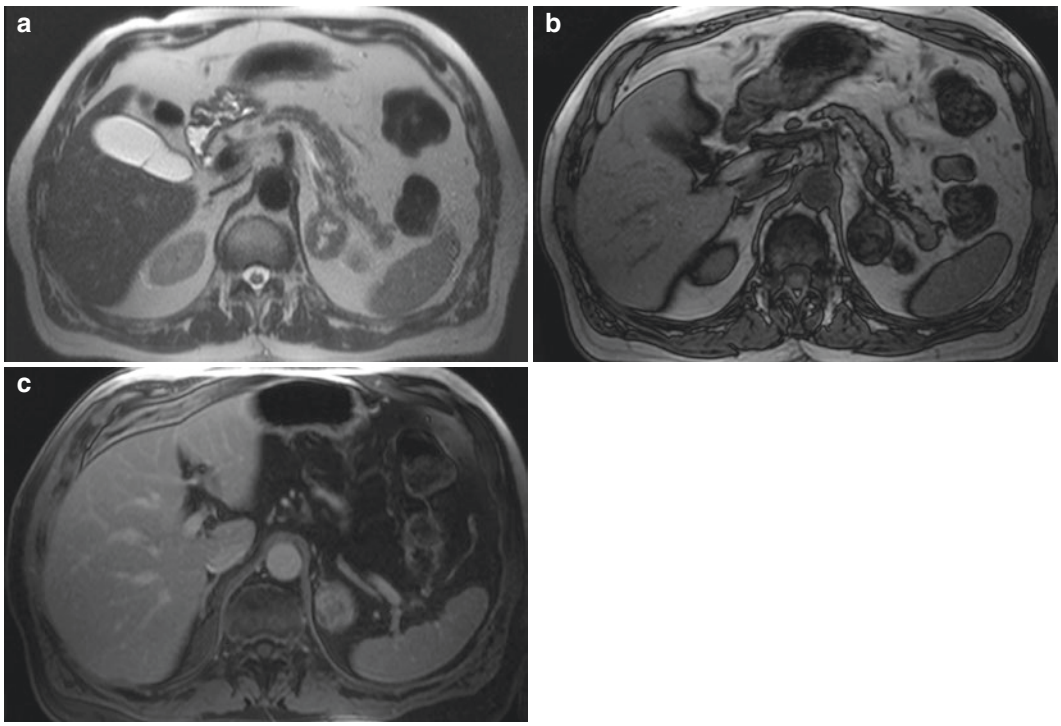

Fig. 5.22 Adrenal cortical adenoma, radioimages. (**a**) CT (T1-weighted image) precontrast images show a heterogeneous focal lesion arising from the left adrenal gland. (**b**) CT scan (out-of-phase image) shows signal dropout in the inferior portion of the lesion; however, the more cranial portion of the lesion demonstrates no significant signal dropout. (**c**) CT (postcontrast) image

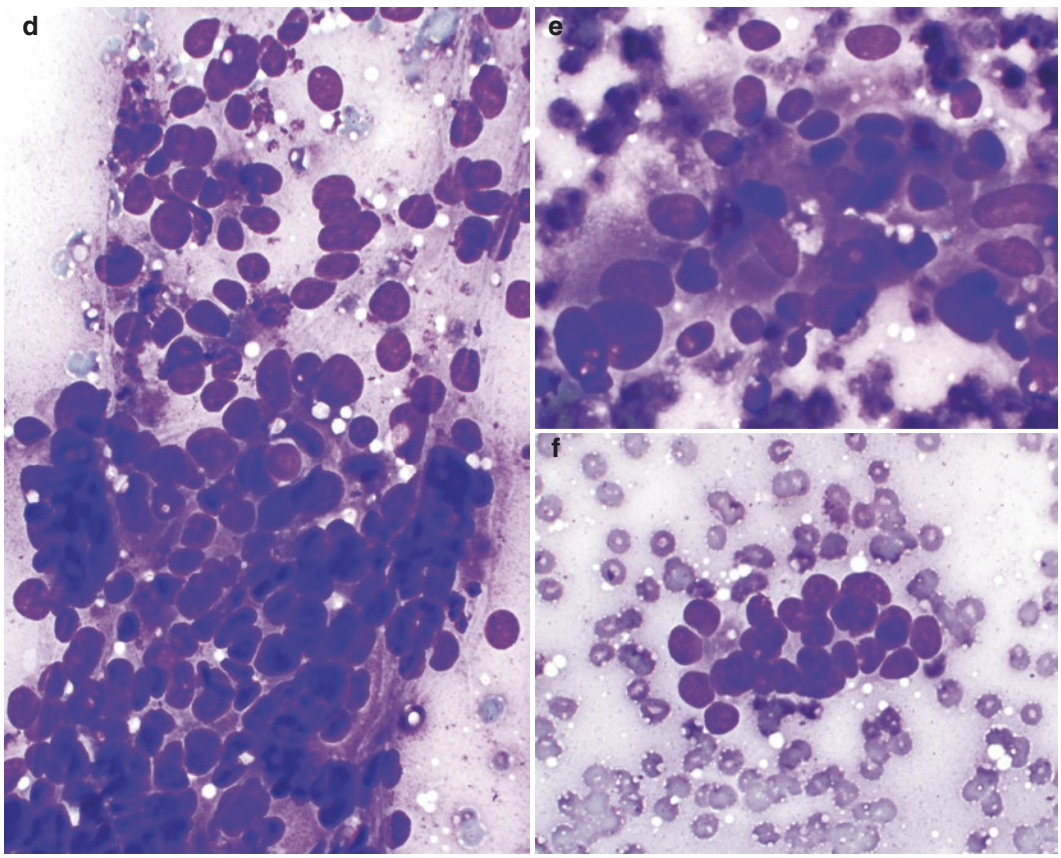

Fig. 5.23 Adrenal cortical adenoma, cytology. FNA biopsy of an adrenal lesion, Diff-Quik stain, 600×

- The nuclei are uniform and round or oval and have granular chromatin and distinct nucleoli [62, 71]. Abundant naked nuclei and intranuclear pseudoinclusions may be present [62, 71]. The cytoplasm is moderate to abundant and clear, delicate, vacuolated, or granular with indistinct cell borders [71]. Marked cytologic atypia may be present.
- A foamy background of lipid droplets is always seen [62].

Comment

1. Differential diagnosis includes non-neoplastic adrenal cortex, nodular hyperplasia, adrenal cortical carcinoma, pheochromocytoma, metastatic RCC, hepatocellular carcinoma, and small blue-cell tumor (when in the presence of aggregates of naked nuclei). It can be very difficult to distinguish cortical adenoma from adrenal cortex tissue and adenocarcinoma by FNA cytology alone. It has been reported that FNA cytology combined with clinical presentation (symptoms and endocrine function) and imaging studies (CT scan, MRI, and norcholesterol scintigraphy) may increase diagnostic accuracy to 100% [56]. However, others have stated that the cytologic features of non-neoplastic adrenal cortical tissue and adenomas are indistinguishable [72].
2. Adrenal cortical adenoma cells are positive for inhibin and melan A while negative for CK7, CK20, and chromogranin.

Primary Adrenal Malignancy

Adrenal Cortical Carcinoma

Clinical

- Frequency is 1–2 cases per 1,00,000/year with a biphasic age distribution [69, 73, 74]; comprise 3% of endocrine neoplasms and 0.02% of all malignant neoplasms [75–77].
- Mean age is 40–50 years [69]. The male-to-female ratio is 1:2.5 [69].
- Eighty percent of adrenal cortical carcinomas are functional (45% glucocorticoid, 45% glucocorticoid and androgen, and 10% androgen alone) [69]. The clinical presentation may vary; some individuals may have symptoms of hyperaldosteronism, virilization, or Cushing syndrome [73, 74, 78].
- Associated syndromes include Li-Fraumeni syndrome, Beckwith-Wiedemann syndrome, and Carney complex.

Radiology

- These masses may have calcification or regions of necrosis and hemorrhage [63].

MRI

- Heterogeneously high T2 signal and possible loss of signal on out-of-phase sequences (Fig. 5.24) [79].

Cytology of FNA and Touch Preparation of Core

- Characteristically, cellular specimen consisting of single and discohesive clusters of bland to highly pleomorphic plasmacytoid or polygonal epithelial cells (Fig. 5.25) [62, 80]. The cells are larger than those of adrenal adenoma [62].
- The nuclei may be eccentrically located and variably enlarged and contain hyperchromatic chromatin and inconspicuous to prominent nucleoli [62, 80]. Nuclear pleomorphism, bizarre-shaped nuclei, binucleation or multinucleation, spindle-shaped nuclei, and occasional naked nuclei can be seen [62, 80]. A variable number of mitoses, including atypical mitotic figures, are frequently seen [62, 80]. The cytoplasm is moderate to abundant and finely granular or vacuolated [80]. With increasing atypia, the cytoplasmic lipid content tends to decrease [62].
- Necrosis is frequently seen [62, 80]. Lipid drops and neutrophils may also be seen [80].

Comment

- The differential diagnosis includes metastatic RCC, adrenal adenoma, pheochromocytoma, neuroendocrine tumor, metastatic melanoma, and metastatic adenocarcinoma.
- ICH stains: At most focally positive for cytokeratins other than CAM5.2. Common reactive for inhibin, melan-A, and calretinin [72].

Pheochromocytoma

Clinical

- Most common tumor in adrenal medulla.
- Generally associated with clinical symptoms caused by overproduction of catecholamines, intermittent paroxysmal hypertension accompanied by sweating, palpitations, headache, diaphoresis, nervousness, nausea, vomiting, weakness, and abdominal or chest pain.

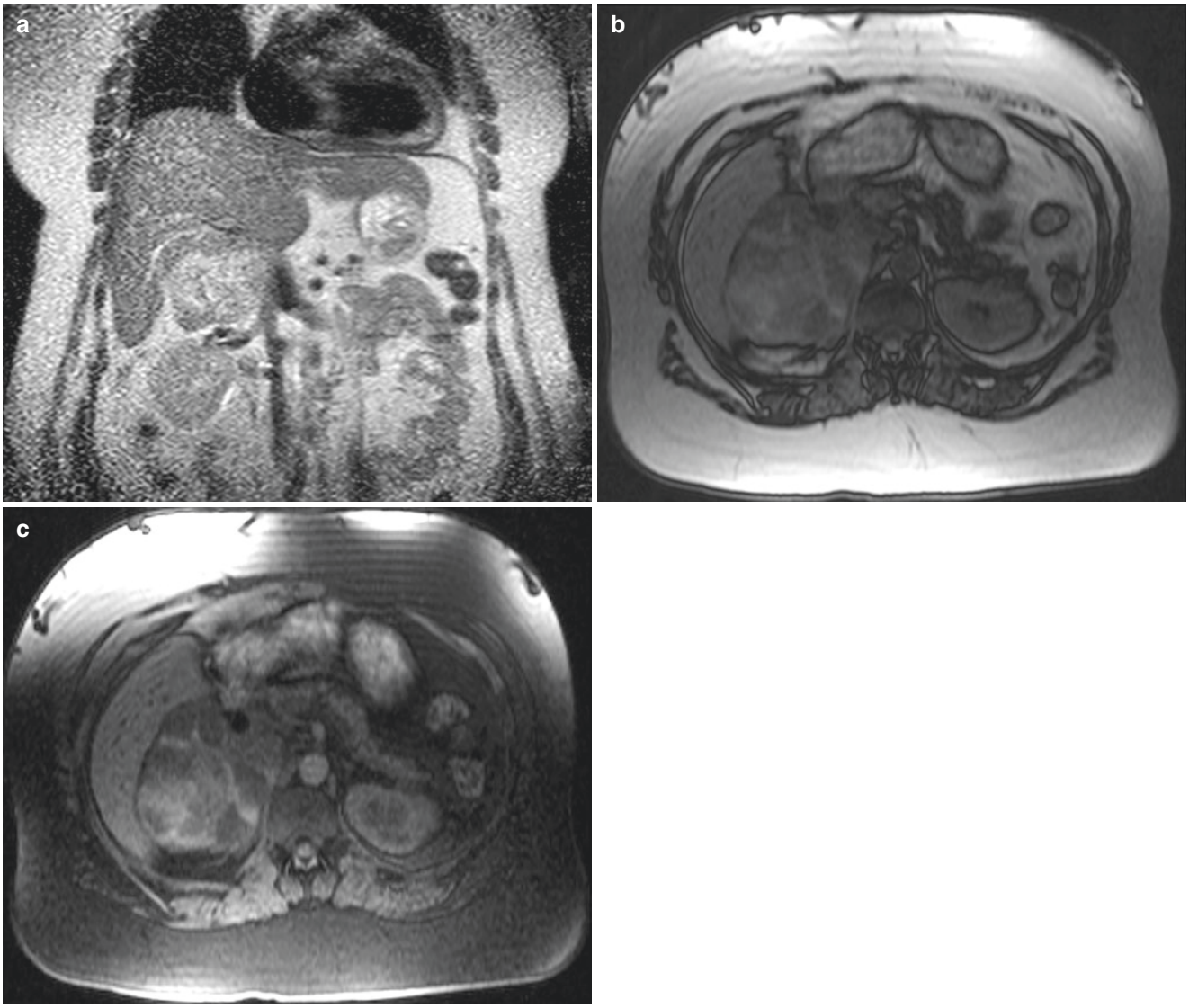

Fig. 5.24 Adrenal carcinoma, radioimage. (**a**) MRI (T1-weighted image) precontrast images show a large heterogeneous mass abutting the liver without evidence of hepatic invasion. The mass is in the expected region of the right adrenal gland. (**b**) MRI (out-of-phase image) shows heterogeneous enhancement with an overall loss of signal intensity. (**c**) MRI (postcontrast image) shows heterogeneous enhancement

Cytology of FNA and Touch Preparation of Core

- FNA findings of pheochromocytoma are similar to those of paraganglioma (*see* paraganglioma below in this chapter). Characteristically, bland to pleomorphic epithelioid or spindle cells; seen singly or in discohesive nests (zellballen) and acinar-microglandular structures or rosettes similar to those seen in paraganglioma (below) (Fig. 5.26) [81].
- The cells have single or multiple eccentrically located (plasmacytoid) round to oval nuclei with prominent nucleoli and granular chromatin [81]. Large intranuclear inclusions, binucleation or multinucleation, and naked nuclei are commonly seen [81]. The cytoplasm is abundant and is delicate, granular, or "squamoid" with ill-defined cell borders [81]. Hyaline globules and rarely melanin pigment may be seen in the cytoplasm [82].
- In cell blocks, characteristic nesting of the tumor cells (zellballen pattern) may be seen.

Comment

- Differential diagnosis: adrenal cortex neoplasm, metastatic adenocarcinoma, melanoma, and neuroendocrine neoplasms.
- Tumor cells are positive for chromogranin, synaptophysin, and NSE and negative for EMA and cytokeratins [72]. Sustentacular cells are positive for S-100.

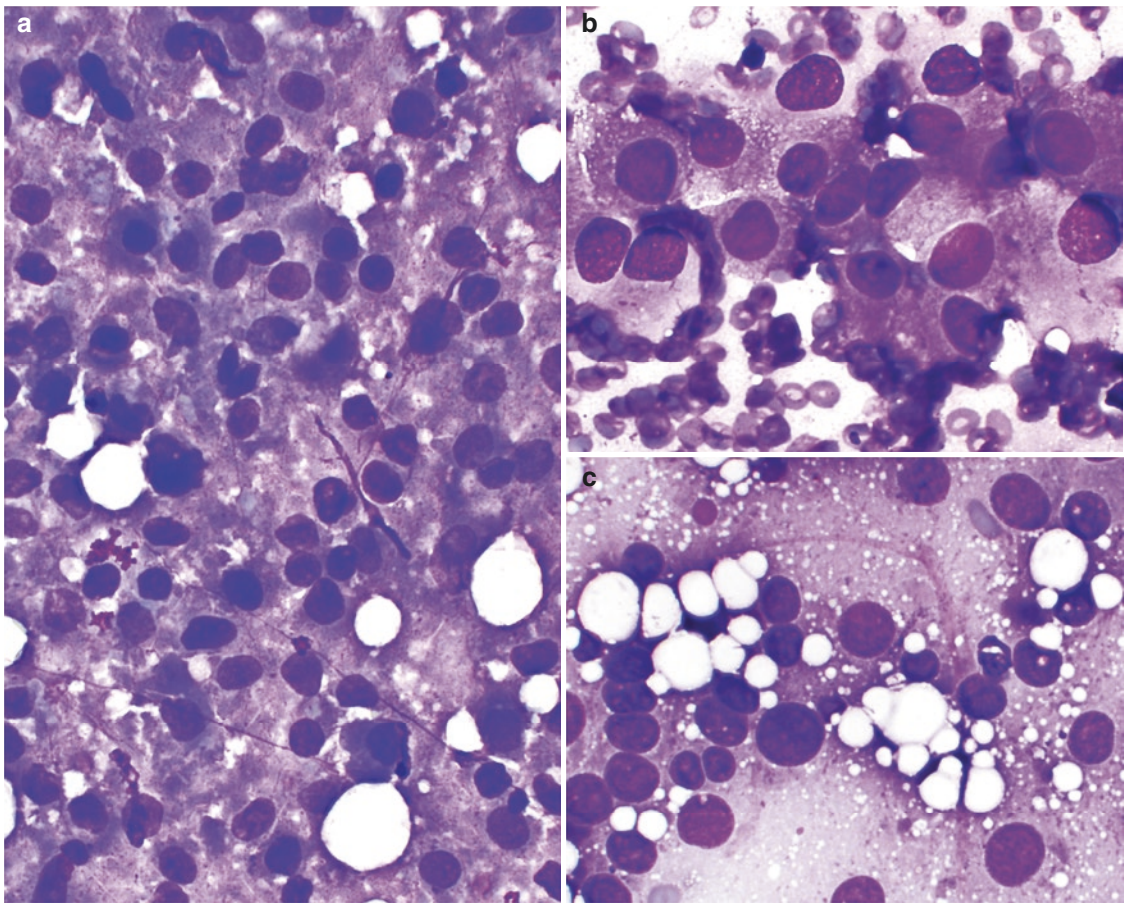

Fig. 5.25 Adrenal cortical carcinoma, cytology. FNA biopsy of a large adrenal mass; Diff-Quik stain, 600×

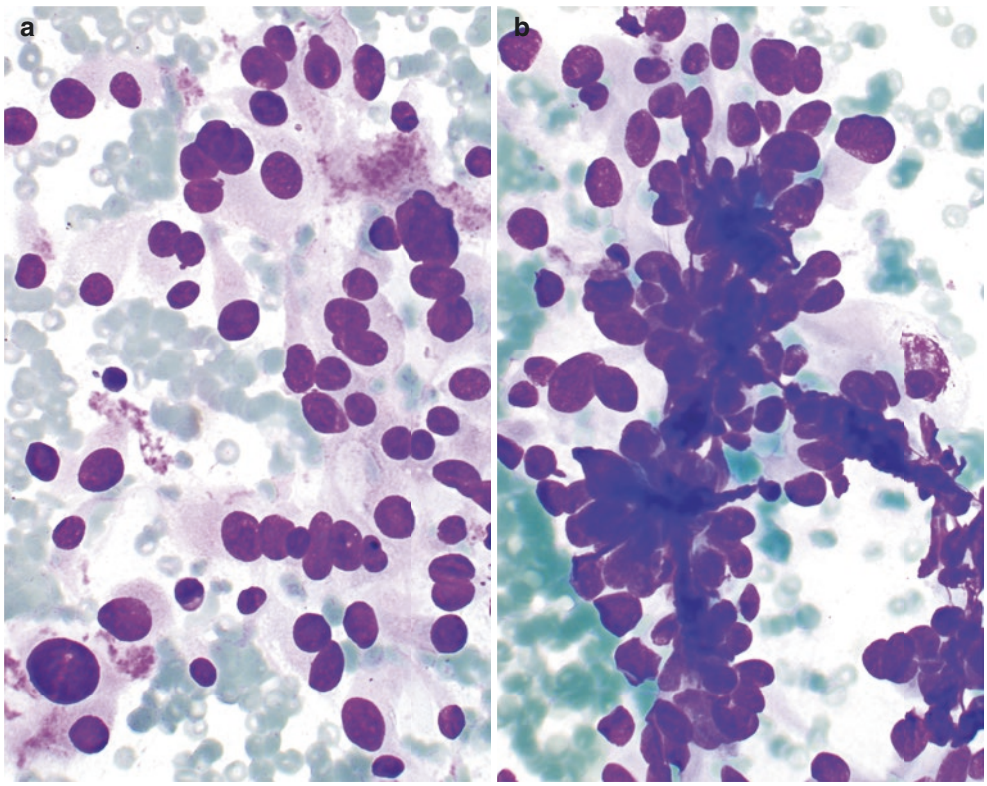

Fig. 5.26 Paraganglioma, cytology. FNA biopsy of a 3-cm retroperitoneal mass; Diff-Quik stain, 600×

- FNA biopsy should be used with caution in cases suspicious for pheochromocytoma owing to possible fatal hypertensive crisis or hemorrhage; therefore biochemical testing for pheochromocytoma should be performed before biopsy of adrenal masses.

Metastatic Malignancy

Clinical

- There is a wide range of stated prevalence of adrenal metastatic disease within adrenal incidentalomas, ranging from 2% to 30% depending on certain risk factors such as a pre-existing cancer diagnosis [63]. Metastatic malignancies are far more common than primary malignancies of the adrenal gland [83]. The adrenal is the fourth most frequent site of spread of tumors after the lungs, liver, and bone [83, 84]. Carcinomas are the most common tumor type to metastasize to the adrenal glands followed by lymphomas and melanoma [85]. Adrenal metastases are found in 27% of patients dying with carcinomas [83, 86].
- The most common primary sites are the breast, lung, kidney, stomach, pancreas, ovary, and colon [83].
- Lymphomatous involvement of the adrenal glands is an uncommon occurrence. Secondary lymphoma of the adrenal is more common than primary lymphoma, which is defined as being found only within the adrenal gland [87].

Radiology

- It is of note that the imaging features of metastatic disease are nonspecific, and that it is essential to take the patient's clinical history into consideration.
- The distribution (bilateral) and size of the lesions (>3 cm) may increase the likelihood of their being metastatic in nature [88].
- Imaging findings in lymphoma can be both discrete and diffuse. On CT evaluation, discrete lymphomatous lesions are mildly enhancing and homogeneous. Diffuse involvement of the adrenal gland may present on imaging as enlargement caused by infiltrative disease [87]. However, these classic findings are not always present, and there is significant variability in CT findings, especially in the setting of primary lymphoma [89].

Cytology of FNA and Touch Preparation of Core

- FNA and CNB are important tools to diagnose adrenal metastases.
- FNA findings vary depending on metastatic malignancies. Morphologic comparison with any known primary malignancy should be performed.

Comment

- IHC stains are very useful in differential diagnosis. Adrenal tumors are positive for melan-A and inhibin and negative for epithelial membrane antigen and keratins.

Paraganglia

Paraganglioma

Clinical

- Uncommon.
- Locations: distribution along the parasympathetic or sympathetic chains or nerves or outside the usual distribution of sympathetic and parasympathetic paraganglia, such as in the bladder, carotid body, central nervous system, gallbladder, and middle ear.
- The "ten rule": 10% are extra-adrenal, 10% are bilateral, 10% are extra-abdominal, 10% are familial (VHL, NF 1, MEN 2A/2B), 10% are pediatric, 10% are not associated with hypertension, and 10% are malignant.
- FNA should be carefully performed because of possible development of a hypertensive episode during the FNA procedure [81].

Cytology of FNA and Touch Preparation of Core

- FNA findings are similar to those of adrenal pheochromocytoma.
- Characteristic presence of single or discohesive groups of cells showing size and shape pleomorphism, forming sheets, acinar-microglandular, zellballen-type, and perivascular patterns (Fig. 5.26) [81, 90, 91].
- The cells may be round, oval, plasmacytoid, or spindled [91]. The cytoplasm is moderate to abundant and vacuolated, finely granular or "squamoid" with ill-defined cell borders [81, 90–93]. Intracytoplasmic metachromatic granules and melanin-like pigment can be seen. The nuclei are round to oval and eccentrically located with "salt and pepper" chromatin and may have prominent nucleoli [81, 90, 93]. Binucleation, multinucleation, intranuclear pseudoinclusions, nuclear grooves, and naked nuclei are commonly seen [81, 90]. Mitotic figures are more frequently seen in malignant cases [91, 92].

Comment

- Tumor cells are positive for chromagranin A, NSE, synaptophysin, and HepPar-1 (11%), while they are negative for EMA and cytokeratins. Sustentacular cells are positive for S-100.

References

1. Garcia-Solano J, Acosta-Ortega J, Perez-Guillermo M, Benedicto-Orovitg JM, Jimenez-Penick FJ. Solid renal masses in adults: image-guided fine-needle aspiration cytology and imaging techniques–"two heads better than one?". Diagn Cytopathol. 2008;36:8–12.
2. Schmidbauer J, Remzi M, Memarsadeghi M, Haitel A, Klingler HC, Katzenbeisser D, et al. Diagnostic accuracy of computed tomography-guided percutaneous biopsy of renal masses. Eur Urol. 2008;53:1003–1.
3. Zardawi IM. Renal fine needle aspiration cytology. Acta Cytol. 1999;43:184–90.
4. Andonian S, Okeke Z, Vanderbrink BA, Okeke DA, Sugrue C, Wasserman PG, et al. Aetiology of non-diagnostic renal fine-needle aspiration cytologies in a contemporary series. BJU Int. 2008;103(1):28–32.
5. Raso DS, Greene WB, Finley JL, Silverman JF. Morphology and pathogenesis of Liesegang rings in cyst aspirates: report of two cases with ancillary studies. Diagn Cytopathol. 1998;19:116–9.
6. Truong LD, Todd TD, Dhurandhar B, Ramzy I. Fine-needle aspiration of renal masses in adults: analysis of results and diagnostic problems in 108 cases. Diagn Cytopathol. 1999;20:339–49.
7. Todd TD, Dhurandhar B, Mody D, Ramzy I, Truong LD. Fine-needle aspiration of cystic lesions of the kidney. Morphologic spectrum and diagnostic problems in 41 cases. Am J Clin Pathol. 1999;111:317–28.
8. Sahni VA, Ly A, Silverman SG. Usefulness of percutaneous biopsy in diagnosing benign renal masses that mimic malignancy. Abdom Imaging. 2011;36:91–101.
9. Katabathina VS, Vikram R, Nagar AM, Tamboli P, Menias CO, Prasad SR. Mesenchymal neoplasms of the kidney in adults: imaging spectrum with radiologic-pathologic correlation. Radiographics. 2010;30:1525–40.
10. Jinzaki M, Silverman SG, Akita H, Nagashima Y, Mikami S, Oya M. Renal angiomyolipoma: a radiological classification and update on recent developments in diagnosis and management. Abdom Imaging. 2014;39:588–604.
11. Kennelly MJ, Grossman HB, Cho KJ. Outcome analysis of 42 cases of renal angiomyolipoma. J Urol. 1994;152(6 Pt 1):1988–91.
12. Steiner MS, Goldman SM, Fishman EK, Marshall FF. The natural history of renal angiomyolipoma. J Urol. 1993;150:1782–6.
13. Tong YC, Chieng PU, Tsai TC, Lin SN. Renal angiomyolipoma: report of 24 cases. Br J Urol. 1990;66:585–9.
14. Hindman N, Ngo L, Genega EM, Melamed J, Wei J, Braza JM, et al. Angiomyolipoma with minimal fat: can it be differentiated from clear cell renal cell carcinoma by using standard MR techniques? Radiology. 2012;265:468–77.
15. Crapanzano JP. Fine-needle aspiration of renal angiomyolipoma: cytological findings and diagnostic pitfalls in a series of five cases. Diagn Cytopathol. 2005;32:53–7.
16. Masoom S, Venkataraman G, Jensen J, Flanigan RC, Wojcik EM. Renal FNA-based typing of renal masses remains a useful adjunctive modality: evaluation of 31 renal masses with correlative histology. Cytopathology. 2009;20:50–5.
17. Cristallini EG, Paganelli C, Bolis GB. Role of fine-needle aspiration biopsy in the assessment of renal masses. Diagn Cytopathol. 1991;7:32–5.
18. Lieber MM. Renal oncocytoma. Urol Clin North Am. 1993;20:355–9.
19. Perez-Ordonez B, Hamed G, Campbell S, Erlandson RA, Russo P, Gaudin PB, et al. Renal oncocytoma: a clinicopathologic study of 70 cases. Am J Surg Pathol. 1997;21:871–83.
20. Hes O, Moch H, Reuter VE. Oncocytoma. In: Moch H, Humphrey PA, Ulbright TM, Reuter VE, editors. WHO classification of tumours of the urinary system and male genital organs. Lyon: International Agency for Research on Cancer; 2016. p. 43–4.
21. Wu J, Zhu Q, Zhu W, Chen W, Wang S. Comparative study of CT appearances in renal oncocytoma and chromophobe renal cell carcinoma. Acta Radiol. 2016;57:500–6.
22. Liu J, Fanning CV. Can renal oncocytomas be distinguished from renal cell carcinoma on fine-needle aspiration specimens? A study of conventional smears in conjunction with ancillary studies. Cancer. 2001;93:390–7.
23. Bishop JA, Hosler GA, Kulesza P, Erozan YS, Ali SZ. Fine-needle aspiration of renal cell carcinoma: is accurate Fuhrman grading possible on cytologic material? Diagn Cytopathol. 2011;39:168–71.
24. Zhu B, Rohan SM, Lin X. Immunoexpression of napsin A in renal neoplasms. Diagn Pathol. 2015;10:4.
25. Zhou M, Roma A, Magi-Galluzzi C. The usefulness of immunohistochemical markers in the differential diagnosis of renal neoplasms. Clin Lab Med. 2005;25:247–57.
26. Lin X. Cytomorphology of clear cell papillary renal cell carcinoma. Cancer Cytopathol. 2017;125:48–54.
27. Moch H, Humphrey PA, Ulbright TM, Reuter VE. WHO classification of tumours of the urinary system and male genital organs. Lyon: International Agency for Research on Cancer; 2016.
28. Lopez-Beltran A, Carrasco JC, Cheng L, Scarpelli M, Kirkali Z, Montironi R. 2009 update on the classification of renal epithelial tumors in adults. Int J Urol. 2009;16:432–43.
29. Hoffmann NE, Gillett MD, Cheville JC, Lohse CM, Leibovich BC, Blute ML. Differences in organ system of distant metastasis by renal cell carcinoma subtype. J Urol. 2008;179:474–7.
30. Low G, Huang G, Fu W, Moloo Z, Girgis S. Review of renal cell carcinoma and its common subtypes in radiology. World J Radiol. 2016;8:484–500.
31. Cheville JC, Lohse CM, Zincke H, Weaver AL, Blute ML. Comparisons of outcome and prognostic features among histologic subtypes of renal cell carcinoma. Am J Surg Pathol. 2003;27:612–24.
32. Gurel S, Narra V, Elsayes KM, Siegel CL, Chen ZE, Brown JJ. Subtypes of renal cell carcinoma: MRI and pathological features. Diagn Interv Radiol. 2013;19:304–11.
33. Moch H, Amin MB, Argani P, Cheville J, Delahunt B, Martignoni G, Medeiros LJ, Srigley JR, Tan PH, Tickoo SK. Renal cell tumours. In: Moch H, Humphrey PA, Ulbright TM, Reuter VE, editors. WHO classification of tumours of the urinary system and male genital organs. Lyon: International Agency for Research on Cancer; 2016. p. 12–7.
34. Parkin D, Whelan S, Ferlay J, Teppo L, Thomas D. Cancer incidence in five continents. Lyon: IARC Scientific Publications No 155. IARC Press; 2003.
35. Sufrin G, Chasan S, Golio A, Murphy GP. Paraneoplastic and serologic syndromes of renal adenocarcinoma. Semin Urol. 1989;7:158–71.
36. Prasad SR, Humphrey PA, Catena JR, Narra VR, Srigley JR, Cortez AD, et al. Common and uncommon histologic subtypes of renal cell carcinoma: imaging spectrum with pathologic correlation. Radiographics. 2006;26:1795–806; discussion, 806–10.
37. Renshaw AA, Granter SR. Fine needle aspiration of chromophobe renal cell carcinoma. Acta Cytol. 1996;40:867–72.
38. Layfield LJ. Fine-needle aspiration biopsy of renal collecting duct carcinoma. Diagn Cytopathol. 1994;11:74–8.
39. Lin X. Cytomorphology of clear cell papillary renal cell carcinoma. Cancer. 2017;125:48–54.
40. Al-Ahmadie HA, Alden D, Fine SW, Gopalan A, Touijer KA, Russo P, et al. Role of immunohistochemistry in the evaluation of needle core biopsies in adult renal cortical tumors: an ex vivo study. Am J Surg Pathol. 2011;35:949–61.
41. Adeniran AJ, Al-Ahmadie H, Iyengar P, Reuter VE, Lin O. Fine needle aspiration of renal cortical lesions in adults. Diagn Cytopathol. 2010;38:710–5.

42. Grignon DJ, Al-Ahmadie H, Algaba F, Amin MD, Comperat E, Dyrskjot L, Epstein JI, Hansel DE, Knuchel R, Lloreta J, Lopez-Beltran A, McKenney JK, Netto GJ, Paner G, Reuter VE, Shen SS, Van der Kwast T. Urothelial tumours. In: Moch H, Humphrey PA, Ulbright TM, Reuter VE, editors. WHO classification of tumours of the urinary system and male genital organs. Lyon: International Agency for Research on Cancer; 2016. p. 77–98.
43. Raza SA, Sohaib SA, Sahdev A, Bharwani N, Heenan S, Verma H, et al. Centrally infiltrating renal masses on CT: differentiating intrarenal transitional cell carcinoma from centrally located renal cell carcinoma. Am J Roentgenol. 2012;198:846–53.
44. Zhu B, Rohan SM, Lin X. Urine cytomorphology of micropapillary urothelial carcinoma. Diagn Cytopathol. 2013;41:485–91.
45. Lin X, Zhu B, Villa C, Zhong M, Kundu S, Rohan SM, et al. The utility of p63, p40, and GATA-binding protein 3 immunohistochemistry in diagnosing micropapillary urothelial carcinoma. Hum Pathol. 2014;45:1824–9.
46. Argani P, Bruder E, Dehner L, Vujanic GM. Nephroblastic and cystic tumours occurring mainly in children. In: Moch H, Humphrey PA, Ulbright TM, Reuter VE, editors. WHO classification of tumours of the urinary system and male genital organs. Lyon: IARC Press; 2004. p. 48–53.
47. Ravindra S, Kini U. Cytomorphology and morphometry of small round-cell tumors in the region of the kidney. Diagn Cytopathol. 2005;32:211–6.
48. Dey P, Radhika S, Rajwanshi A, Rao KL, Khajuria A, Nijhawan R, et al. Aspiration cytology of Wilms' tumor. Acta Cytol. 1993;37:477–82.
49. Khayyata S, Grignon DJ, Aulicino MR, Al-Abbadi MA. Metanephric adenoma vs. Wilms' tumor: a report of 2 cases with diagnosis by fine needle aspiration and cytologic comparisons. Acta Cytol. 2007;51:464–7.
50. Quijano G, Drut R. Cytologic characteristics of Wilms' tumors in fine needle aspirates. A study of ten cases. Acta Cytol. 1989;33:263–6.
51. Nayak A, Iyer VK, Agarwala S. The cytomorphologic spectrum of Wilms tumour on fine needle aspiration: a single institutional experience of 110 cases. Cytopathology. 2011;22:50–9.
52. Aras M, Dede F, Ones T, Inanir S, Erdil TY, Turoglu HT. Is the value of FDG PET/CT in evaluating renal metastasis underestimated? A case report and review of the literature. Mol Imaging Radionuc Ther. 2013;22:109–12.
53. Shimko MS, Jacobs SC, Phelan MW. Renal metastasis of malignant melanoma with unknown primary. Urology. 2007;69:384.e9–10.
54. Israel GM, Bosniak MA. Pitfalls in renal mass evaluation and how to avoid them. Radiographics. 2008;28:1325–38.
55. Quayle FJ, Spitler JA, Pierce RA, Lairmore TC, Moley JF, Brunt LM. Needle biopsy of incidentally discovered adrenal masses is rarely informative and potentially hazardous. Surgery. 2007;142:497–502; discussion, 502–4.
56. Lumachi F, Borsato S, Tregnaghi A, Marino F, Fassina A, Zucchetta P, et al. High risk of malignancy in patients with incidentally discovered adrenal masses: accuracy of adrenal imaging and image-guided fine-needle aspiration cytology. Tumori. 2007;93:269–74.
57. Nurnberg D. Ultrasound of adrenal gland tumours and indications for fine needle biopsy (uFNB). Ultraschall Med. 2005;26:458–69.
58. Bovio S, Cataldi A, Reimondo G, Sperone P, Novello S, Berruti A, et al. Prevalence of adrenal incidentaloma in a contemporary computerized tomography series. J Endocrinol Investig. 2006;29:298–302.
59. Herrera MF, Grant CS, van Heerden JA, Sheedy PF, Ilstrup DM. Incidentally discovered adrenal tumors: an institutional perspective. Surgery. 1991;110:1014–21.
60. Tikkakoski T, Taavitsainen M, Paivansalo M, Lahde S, Apaja-Sarkkinen M. Accuracy of adrenal biopsy guided by ultrasound and CT. Acta Radiol. 1991;32:371–4.
61. Lumachi F, Borsato S, Tregnaghi A, Basso SM, Marchesi P, Ciarleglio F, et al. CT-scan, MRI and image-guided FNA cytology of incidental adrenal masses. Eur J Surg Oncol. 2003;29:689–92.
62. Fassina AS, Borsato S, Fedeli U. Fine needle aspiration cytology (FNAC) of adrenal masses. Cytopathology. 2000;11:302–11.
63. Lattin GE, Sturgill ED, Tujo CA, Marko J, Sanchez-Maldonado KW, Craig WD, et al. From the radiologic pathology archives: adrenal tumors and tumor-like conditions in the adult: radiologic-pathologic correlation. Radiographics. 2014;34:805–29.
64. Olsson CA, Krane RJ, Klugo RC, Selikowitz SM. Adrenal myelolipoma. Surgery. 1973;73:665–70.
65. Kenney PJ, Wagner BJ, Rao P, Heffess CS. Myelolipoma: CT and pathologic features. Radiology. 1998;208:87–95.
66. Lam KY, Lo CY. Adrenal lipomatous tumours: a 30 year clinicopathological experience at a single institution. J Clin Pathol. 2001;54:707–12.
67. Settakorn J, Sirivanichai C, Rangdaeng S, Chaiwun B. Fine-needle aspiration cytology of adrenal myelolipoma: case report and review of the literature. Diagn Cytopathol. 1999;21:409–12.
68. Stewart PM. The adrenal cortex. In: Larsen PR, Kronenberg HM, Melmed S, Polonsky KS, editors. Williams textbook of endocrinology. 10th ed. Philadelphia: WB Saunders; 2002. p. 491–551.
69. Lloyd RV, Osamura RY, Kloppel G, Rosai J. Tumours of the adrenal cortex. In: Lloyd RV, Osamura RY, Kloppel G, Rosai J, editors. WHO classification of Tumours of endocrine organs. Lyon: International Agency for Research on Cancers; 2016. p. 161–78.
70. Elsayes KM, Mukundan G, Narra VR, Lewis JS, Shirkhoda A, Farooki A, et al. Adrenal masses: MR imaging features with pathologic correlation. Radiographics. 2004;24(Suppl 1):S73–86.
71. Stelow EB, Debol SM, Stanley MW, Mallery S, Lai R, Bardales RH. Sampling of the adrenal glands by endoscopic ultrasound-guided fine-needle aspiration. Diagn Cytopathol. 2005;33:26–30.
72. Jorda M, De MB, Nadji M. Calretinin and inhibin are useful in separating adrenocortical neoplasms from pheochromocytomas. Appl Immunohistochem Mol Morphol. 2002;10:67–70.
73. Allolio B, Fassnacht M. Clinical review: Adrenocortical carcinoma: clinical update. J Clin Endocrinol Metab. 2006;91:2027–37.
74. Wooten MD, King DK. Adrenal cortical carcinoma. Epidemiology and treatment with mitotane and a review of the literature. Cancer. 1993;72:3145–55.
75. Schteingart DE, Doherty GM, Gauger PG, Giordano TJ, Hammer GD, Korobkin M, et al. Management of patients with adrenal cancer: recommendations of an international consensus conference. Endocr Relat Cancer. 2005;12:667–80.
76. Roman S. Adrenocortical carcinoma. Curr Opin Oncol. 2006;18:36–42.
77. Ng L, Libertino JM. Adrenocortical carcinoma: diagnosis, evaluation and treatment. J Urol. 2003;169:5–11.
78. Venkatesh S, Hickey RC, Sellin RV, Fernandez JF, Samaan NA. Adrenal cortical carcinoma. Cancer. 1989;64:765–9.
79. Bharwani N, Rockall AG, Sahdev A, Gueorguiev M, Drake W, Grossman AB, et al. Adrenocortical carcinoma: the range of appearances on CT and MRI. Am J Roentgenol. 2011;196:W706–14.
80. Ren R, Guo M, Sneige N, Moran CA, Gong Y. Fine-needle aspiration of adrenal cortical carcinoma: cytologic spectrum and diagnostic challenges. Am J Clin Pathol. 2006;126:389–98.
81. Jimenez-Heffernan JA, Vicandi B, Lopez-Ferrer P, Gonzalez-Peramato P, Perez-Campos A, Viguer JM. Cytologic features of pheochromocytoma and retroperitoneal paraganglioma: a morphologic and immunohistochemical study of 13 cases. Acta Cytol. 2006;50:372–8.
82. Handa U, Khullar U, Mohan H. Pigmented pheochromocytoma: report of a case with diagnosis by fine needle aspiration. Acta Cytol. 2005;49:421–3.

83. Lloyd RV, Kawashima A, Tischler AS. Secondary tumors. In: DeLellis RA, Lloyd RV, Heitz PU, Eng C, editors. Pathology and genetics: tumors of endocrine organs. Lyon: IARC Press; 2004. p. 172–3.
84. Willis RV. The spread of tumors in the human body. 3rd ed. London: Butterworth; 1973.
85. Mayo-Smith WW, Boland GW, Noto RB, Lee MJ. State-of-the-art adrenal imaging. Radiographics. 2001;21:995–1012.
86. Abrams HL, Spiro R, Goldstein N. Metastases in carcinoma; analysis of 1000 autopsied cases. Cancer. 1950;3:74–85.
87. Leite NP, Kased N, Hanna RF, Brown MA, Pereira JM, Cunha R, et al. Cross-sectional imaging of extranodal involvement in abdominopelvic lymphoproliferative malignancies. Radiographics. 2007;27:1613–34.
88. Chong S, Lee KS, Kim HY, Kim YK, Kim BT, Chung MJ, et al. Integrated PET-CT for the characterization of adrenal gland lesions in cancer patients: diagnostic efficacy and interpretation pitfalls. Radiographics. 2006;26:1811–24; discussion, 24–6.
89. Rashidi A, Fisher SI. Primary adrenal lymphoma: a systematic review. Ann Hematol. 2013;92:1583–93.
90. Gong Y, DeFrias DV, Nayar R. Pitfalls in fine needle aspiration cytology of extraadrenal paraganglioma. A report of 2 cases. Acta Cytol. 2003;47:1082–6.
91. Varma K, Jain S, Mandal S. Cytomorphologic spectrum in paraganglioma. Acta Cytol. 2008;52:549–56.
92. Absher KJ, Witte DA, Truong LD, Ramzy I, Mody DR, Ostrowski ML. Aspiration biopsy of osseous metastasis of retroperitoneal paraganglioma. Report of a case with cytologic features and differential diagnostic considerations. Acta Cytol. 2001;45:249–53.
93. Rana RS, Dey P, Das A. Fine needle aspiration (FNA) cytology of extra-adrenal paragangliomas. Cytopathology. 1997;8:108–13.